

**Design and Optimization of Multiple Printed Inverted-F
Antennas (PIFAs) on a Semi-Populated Mobile Handset**

Ashar Jamil Wahidi

Department of Electrical and Computer Engineering

McGill University

Montreal, Quebec, Canada

August 2012

A thesis submitted to McGill University in partial fulfillment of the requirements for
the degree of Master of Engineering

© 2012 Ashar Jamil Wahidi

Abstract

This thesis investigates the radiation characteristics of a semi-populated cellular mobile handset that uses two Printed Inverted-F Antennas (PIFAs). The investigation is carried out at three different frequencies; the LTE Band 13 (746-786 MHz), GSM-900 (890-960 MHz) and GSM-1800 (1710-1880 MHz). The mobile handset is populated with the components that affect the antenna properties the most, a battery and an LCD screen, to make the investigated model more realistic. A methodology is first presented to design the PIFAs in the presence of other components on the board. Using the outlined method, antennas for three semi-populated mobile handsets are designed to satisfy specific operational performance targets. The two PIFAs fabricated for the GSM-1800 handset have a maximum gain of 2.98 dB and 3.18 dB, reflection coefficients of below -9 dB and a maximum mutual coupling of -7.9 dB. The two fabricated PIFAs of the GSM-900 handset exhibit a maximum gain of -0.02 dB and -3 dB, reflection coefficients of below -10.5 dB and a maximum mutual coupling of -6 dB. The measured gain values for the two PIFAs of LTE-Band 13 handset prototype are 0.19 dB and -11 dB, while both achieving reflection coefficients of below -4.5 dB and a maximum mutual coupling of -11 dB. The three designs all indicate that the presence of the components on the handset

degrade radiation performance. The three handsets nevertheless are well designed to meet all the performance targets except for the mutual coupling.

Fullwave pointing vector simulations are conducted to investigate the coupling between the PIFAs showing that the power transfer between the GSM-1800 and GSM-900 PIFAs mostly takes place through radiation. The power coupled between the LTE-Band 13 handset antennas on the other hand is majorly through the handset's structure and substrate-bound modes.

A survey of different mutual coupling reduction techniques is presented. A method that targets coupling through space-waves, i.e., the use of a parasitic radiator, is applied in this work to the GSM-1800 and GSM-900 handsets. The parasitic radiator succeeds in bringing the maximum coupling between the GSM-1800 handset antennas to below -18 dB and below -17.5 dB for the GSM-900 handset antennas. The mutual coupling between the LTE-Band 13 handset antennas is reduced by using an Electromagnetic Band-Gap structure, which successfully decreases it to below -12.2 dB.

Abstrait

Cette thèse analyse les caractéristiques des radiations d'un téléphone mobile cellulaire semi-peuplé utilisant deux antennes imprimées en F-inversé (PIFAs). L'enquête est réalisée à trois fréquences différentes; la bande LTE 13 (746-786 MHz), GSM-900 (890-960 MHz) et GSM-1800 (1710-1880 MHz). Le téléphone mobile est constitué d'une batterie et d'un écran LCD dont le but est de rendre le modèle étudié plus réaliste. Le modèle utilisé vise d'abord à représenter la conception des PIFAs et ceci avec d'autres composants. Par référence à la méthode de conception qui a été décrite, les antennes de trois semi-peuplées téléphones mobiles sont conçus pour satisfaire des objectifs spécifiques de performance opérationnelle. Les deux PIFAs fabriqués pour les mobiles GSM-1800 ont un gain maximal de 2.98 dB and 3.18 dB, coefficients de réflexion inférieur à -9 dB et un couplage maximal mutuel des -7.9 dB. De plus, les deux PIFAs fabriqués pour les mobiles GSM-900 ont un gain maximal de -0.02 dB and -3 dB, coefficients de réflexion ci-dessous -10.5 dB et un couplage maximal mutuel de -6 dB. Enfin, les deux PIFAs fabriqués pour les mobiles LTE-Band 13 atteignent un gain maximal de 0.19 dB and -11 dB, un coefficient de réflexion ci-dessous -4.5 dB et un couplage maximal mutuel de -11 dB.

Les trois modèles indiquent que la présence d'autres composants provoquent la dégradation des performances des radiations. Néanmoins, les

trois mobiles répondent à toutes les caractéristiques de rendement sauf celui pour le couplage mutuel.

Des simulation utilisant des vecteurs pleine-onde pointant sont effectuées pour investiguer le couplage entre les PIFAs. Les simulations indiquent que le tranfert de la puissance couplée entre les antennes pour les mobiles GSM-1800 et GSM-900 se déroule en dehors du mobile. Alors que la puissance couplée entre les antennes de téléphones LTE-bande 13 se fait à travers la structure et le substrat-lié du mobile.

Une récapitulation des différentes techniques de réduction des couplages mutuels a été présentée. Une méthode visant les ondes spatiales i.e., utilisation d'un radiateur parasite, est appliquée aux mobiles GSM 1800 et GSM--900. Le radiateur parasite parvient à rendre le couplage maximal, pour les antennes GSM-1800, au-dessous de -18 dB et pour les antennes GSM-900 au-dessous de -17,5 dB.

Le couplage mutuel de la LT-bande 13 est réduite en utilisant une structure de bande-interdite électromagnétique, qui apporte avec succès le couplage maximal mutuel pour les antennes à moins de -12,2 dB.

En conclusion, la structure PIFA est une option viable pour une utilisation d'un téléphone mobile pour les bandes de fréquences d'une enquête, et ceci en appliquant les techniques de réduction mutuelles de couplage appropriées.

Acknowledgments

I would like to thank my supervisor, Prof. Ramesh Abhari, for the opportunity to work with her and her group at the Integrated Microsystems Laboratory, McGill University. Prof. Abhari's infinite reserves of encouragement, regular and meaningful meeting sessions and her able guidance have helped make my journey through this degree an enjoyable one. I would also like to thank my co-supervisor, Dr. Shirook M. H. Ali, of the Advanced Technology Team at Research In Motion, for the opportunity to collaborate with her on research problems that have immediate practical applications. I benefitted immensely from Dr. Ali's industrial research experience and wish to thank her for the opportunity to work with her group over the summer of 2012 in Waterloo. I could not have asked for two better people to help guide me through this degree, and I will remain obliged to both of them for their valuable insights and inputs.

I would like to thank my colleagues: Mr. Kasra Payandehjoo, Mr. Abdulhadi E. Abdulhadi, Mr. Mohammad Shahidzadeh Mahani and Dr. Hamidreza Memarzadeh. The environment they have set up in the Integrated Circuits and Systems Laboratory is both friendly and academic. Working alongside them was a pleasure.

I would like to extend my gratitude to my friends here in Montreal; Mr. Kamal Farah, Mr. Kanishka Jayawardene and Mr. Sultan Ali Ahmed. I must thank Ms. Stephanie Aoun for help with translating the abstract. I would also like to thank my friends outside of Montreal: Mr. Zubair Khan, Mr. Sheraz Malik, Mr. Haseebullah Khan and Mr. Basil Baqai. I would also like to thank Mr. Muhammad Tenzeem-ur-Rehman and his family for the hospitality and generosity that they extended to me during my degree.

Finally, and most important of all, I would like to thank my family. My parents, Dr. Khalid Jamil and Mrs. Farhat Fatma, for their love and for instilling in me the burning desire to satisfy my infinite curiosity, and my sister, Ms. Anam Wahidi, for always being a constant pillar of support. I would not be who I am if it were not for them.

Contents

Abstract	1
Abstrait	3
Acknowledgments	5
Contents	7
List of Tables	10
List of Figures	11
List of Acronyms	16
Chapter 1	17
Introduction	17
1.1 Background	17
1.2 Thesis Motivation	22
1.3 Thesis Contributions.....	25
1.4 Thesis Outline	26
Chapter 2	28
Printed Inverted-F Antennas (PIFA) on a Semi-Populated Mobile Handset	28
2.1 Introduction	28
2.2 Methodology to Design a PIFA	29
2.3 The Design and Analysis of a PIFA for a Mobile Handset.....	33

2.3.1 PIFA for GSM-1800	37
2.3.2 PIFA for GSM-900	44
2.3.3 PIFA for LTE-Band 13.....	52
2.4 Conclusion	65
Chapter 3	67
Mutual Coupling Between Two Antennas on a Semi-Populated Handset.....	67
3.1 The Definition of Mutual Coupling.....	67
3.2 The Factors Responsible for Mutual Coupling	69
3.3 Simulation Setup	71
3.4 Results	75
3.4 Conclusion	77
Chapter 4	78
Mutual Coupling Reduction Techniques	78
4.1 Introduction	78
4.2 Overview of Mutual Coupling Reduction Techniques.....	79
4.3 Mutual Coupling Reduction Techniques for a Mobile Handset.....	82
4.4 Investigation of Antenna Coupling Reduction Techniques in a Semi-Populated Handset.....	86
4.4.1 Investigation of a Bent Monopole Parasitic Radiator for a Mobile Handset.....	86

4.4.2 Investigation of a Ground Slot Parasitic Radiator for a Mobile Handset	93
4.4.3 Investigation of Electromagnetic Band-Gap Structures for coupling reduction in a Mobile Handset	96
4.5 Conclusion	106
Chapter 5	108
Conclusion	108
5.1 Thesis Summary	108
5.2 Thesis Conclusions	110
5.3 Future Work	112
References.....	114

List of Tables

Table 2.1 Performance Requirements for the Mobile Handset Antennas.....	36
Table 2.2 Simulated and Measured Performance of Antennas for GSM-1800 Handset.	41
Table 2.3 Simulated and Measured Performance of GSM-900 Handset Antennas.....	49
Table 2.4 Simulated and Measured Performance of LTE-B13 Handset Antennas.....	60
Table 2.5 Dependence of LTE-Band 13 PIFAs on Phase Difference between Antennas.	60
Table 2.6 Simulated and Measured Performance of LTE-Band 13 Handset Antennas in Scenario 2.....	62
Table 2.7 Simulated and Measured Performance of LTE-Band 13 Handset Antennas in Scenario 3.....	62
Table 3.2 Mutual Coupling Profile Simulation Results.	75
Table 4.1 Dimensions of Parasitic Radiator.....	87
Table 4.2 Simulated Performance of Antennas for GSM-900 Handset with and without parasitic radiator.....	93
Table 4.3 Simulated Performance of Antennas for GSM-1800 Handset with and without ground slot radiator	94
Table 4.4 Simulated Performance of Antennas for LTE-B13 Handset with and without EBG structures.....	105
Table 4.5 Dependence of LTE-Band 13 PIFAs with EBG structure on Phase Difference between Antennas.	106

List of Figures

Fig. 1.1 (a) The Motorola DynaTAC with a monopole antenna. Image source: [57] (b) The Nokia 5510 with a helical antenna. Image source: [58] (c) The Sony Ericsson Xperia with the patch antennas visible at the top. Image source: [60].....	18
Fig. 1.2 The populated interior of the BlackBerry Storm. The LCD screen and battery have been removed to show the other on-board systems and antennas. Image source: [59].....	20
Fig. 2.1 : The Printed Inverted-F Antenna. Length, L; Height, H; Radiating Arm width, W; Distance between vertical Radiating Arm and Shorting Arm, D. Note: Thickness of Ground Plane is exaggerated for illustrative purposes.....	30
Fig. 2.2 : The investigated handset (without the antennas) (a)The 3D view of the unpopulated handset. (b) The 3D view of the semi-populated handset (c) Top view with labeled parameters of the semi-populated handset.	34
Dimensions: GW=60, GL =95, H=9, BW= 40, BL=51, SW=45, SL=32, SD=6.5, BD=17.5 (all values in mm)	34
Fig. 2.3 : The GSM-1800 Handset (a) Positioning of the PIFAs on the handset (b) The designed PIFA for GSM-1800 MHz (c) Side view of the Antenna #1 on the fabricated handset (d) 3D view of Antenna#2 on the fabricated GSM-1800 handset.....	38
Dimensions: L=23.5, W=4, H=9, A=13.9, B=4, C=2, D=1.5, E=2 (all units are mm)	38
Fig. 2.4 : The S-Parameter for the Antennas of the GSM-1800 Handset (a) Simulation results (b) Measurement results.	42

Fig. 2.5 : The Radiation Pattern for the semi-populated GSM-1800 handset at 1.8 GHz ($\varphi=0$) (a) Simulation result for Antenna #1 (b) Fabricated result for Antenna #1 (c) Simulation result for Antenna #2 (d) Fabricated result for Antenna #2..... 43

Fig. 2.6 : The GSM-900 Handset (a) Positioning of the PIFAs on the Handset (b) The Designed PIFA for the GSM-900 Handset (c) Side view of Antenna #1 on the fabricated handset (d) 3D view of Antenna #2 on the fabricated handset..... 44

Dimensions: L1=37.8, L2=40, W=6, H=9, A=4, B=32, C=7, D=0.5, E=2; G=3.5, J=2 (All units are mm) 44

Fig. 2.7 : The S-Parameter for the Antennas of the GSM-900 Handset (a) Simulation results (b) Measurement results. 50

Fig. 2.8 : The Radiation Pattern of the semi-populated GSM-900 handset antennas at 925MHz ($\varphi=0$) (a) Simulation result for Antenna #1 (b) Measured result for Antenna #1 (c) Simulation result for Antenna #2 (d) Measured result for Antenna #2..... 51

Fig. 2.9 : The LTE-Band 13 Handset (a) Positioning of the PIFAs on the handset (b) The Designed PIFA for the LTE Band 13 Handset (c) 3D view of the fabricated model showing (c) Antenna#1 and (d) Antenna #2. 53

Dimensions: L1=65, L2=60, W=4.5, H=9, A=2, B=55, C=1, D=1.5, E=1.5; F=1.5 (all units are mm)..... 53

Fig. 2.10: The S-Parameter for the Antennas of the LTE-B13 Handset (a) Simulation results (b) Measurement results. 61

Fig. 2.11 : The Simulated Radiation Patterns of the LTE-Band 13 PIFAs in $\varphi=0$ (red) and $\varphi=90$ (blue)-planes in Scenario 1 when the feeding phase difference is: (a) 0 (b) $\pi/2$ (c) π 62

Fig. 2.12 : The Ground Current Distribution on the LTE-Band 13 Handset (a) When the phase difference is set to zero. (b) When the phase difference is set to 180 degrees....63

Fig. 2.13 : The Radiation Pattern of the semi-populated GSM-900 handset antennas at 925 MHz ($\varphi=0$ plane) (a) Simulation result for Antenna #1 (Scenario 2) (b) Measured result for Antenna #1 (Scenario 2) (c) Simulation result for Antenna #2 (Scenario 3) (d) Measured result for Antenna #2 (Scenario 3).64

Fig. 3.1: The Definition of Scattering Parameters for a two Antenna System.68

Fig. 3.2: The Field Calculator in the Ansoft HFSS Ver. 12 software.....71

Fig. 3.3: The “Handset Cross Section” Area defined for (a) the GSM-900/1800 Models (b) LTE-Band 13 Model.73

Fig. 3.5: The “Space Cross Section” Area defined for the GSM-900/1800 Models (a) The orientation of the Space Cross Section with respect to the handset (b) The Space Cross Section with the handset hidden from view.....74

Fig. 3.4: The “Space Cross Section” Area defined for the GSM-900/1800 Models (a) The orientation of the Space cross section with respect to the handset (b) The Space cross section with the handset hidden from view.74

Fig. 3.6 The Results of the Mutual Coupling Profiles for the three Handsets.76

Fig. 4.1 (a) 3D view of the placement of the parasitic radiator between the two antennas (b) The layout parameters of the parasitic radiator.86

Fig. 4.2 The S-Parameters for (a) GSM-1800 handset with and without parasitic radiator (b) GSM-900 handset with and without parasitic radiator.90

Fig. 4.3: The Radiation Pattern of the semi-populated GSM-1800 handset antennas at 1.8 GHz ($\varphi=0$) (a) Simulation result for Antenna #1 without parasitic radiator (b) Simulation result for Antenna #1 with parasitic radiator (c) Simulation result for Antenna

#2 without parasitic radiator (d) Simulation result for Antenna #2 with parasitic radiator.	91
Fig. 4.4: The Radiation Pattern of the semi-populated GSM-900 handset antennas at 925MHz ($\varphi=0$) (a) Simulation result for Antenna #1 without parasitic radiator (b) Simulation result for Antenna #1 with parasitic radiator (c) Simulation result for Antenna #2 without parasitic radiator (d) Simulation result for Antenna #2 with parasitic radiator.	92
Fig. 4.5 The Parasitic Slot Antenna on the GSM-1800 Handset model.....	93
Fig. 4.6 The S-Parameters of the GSM-1800 Handset antennas with parasitic radiator.	95
Fig. 4.7 : The Unit Cell of an Electromagnetic Band-Gap structure. Thickness of items in side-view exaggerated for illustrative purposes.	96
Fig. 4.9 An example of a metallic shielding box in a mobile handset: the interior of the Apple iPhone 3GS features a metallic shielding box to house the circuit boards. Image source: [72]	97
Fig. 4.8 The generation of capacitive and inductive impedances in the unit cells of a mushroom type EBG structure.	96
Fig. 4.10 The Unit Cell of the Electromagnetic Band Gap Structure for the Mobile Handset.....	98
Fig. 4.11 Geometrical parameters of the unit cell for the GSM-900/LTE-Band 13 Handsets.....	99
Dimensions: DG=0.75, DE=0.2 , DB=0.75, patch length and width=28 (all values in mm)	99
Fig. 4.12 The metallic shielding box and the 3 X 2 EBG array placed below it.....	99

Fig. 4.13 Dispersion diagram for the unit cell of the EBG structure shown in Figure 4.10 for the GSM-900/LTE-B13 Handset..... 100

Fig. 4.14 : The Radiation Pattern for the semi-populated LTE-B13 handset at 766 MHz ($\varphi=0$) (a) Simulation result for Antenna #1 without EBG structure(b) Simulated result for Antenna #1 with EBG structure(c) Simulation result for Antenna #2 without EBG structure (d) Simulation result for Antenna #2 with EBG structure. 103

Fig. 4.15 : The radiation pattern of the semi-populated LTE-B13 handset at 766 MHz ($\varphi=0$) (a) Simulation result for Antenna #1 without EBG structure(b) Simulated result for Antenna #1 with EBG structure(c) Simulation result for Antenna #2 without EBG structure (d) Simulation result for Antenna #2 with EBG structure. 104

Fig. 4.16 : The radiation patterns of the LTE-Band 13 PIFAs at $\varphi=0$ (red) and $\varphi=90$ (blue) planes when the phase difference is: (a) 0 (b) $\pi/2$ (c) π 105

List of Acronyms

2D	Two Dimensional
3D	Three Dimensional
3GPP	3 rd Generation Partnership Project
EBG	Electromagnetic Band Gap
GHz	Gigahertz
GSM	Global System for Mobile Communication
HFSS	High Frequency Structure Simulator
ITU	International Telecommunication Union
LCD	Liquid Crystal Display
LTE	Long Term Evolution
MHz	Megahertz
PCS	Personal Communication System
PIFA	Printed Inverted-F Antenna
RIM	Research In Motion
S-Parameters	Scattering Parameters
WiMAX	Worldwide Interoperability for Microwave Access
WLAN	Wireless Local Area Network

Chapter 1

Introduction

1.1 Background

Since their commercial launch in the 1970s, mobile handsets have evolved to become tools of necessity and leisure. In order to increase the functionality of the handset and yet maintain the physical form that allows for handheld use, manufacturers have continuously faced the design challenge of integrating an increasing number of complex circuits within a set device volume. The focus of mobile handset design has been therefore to decrease system footprint, cost and volume while meeting preset performance metrics set by telecommunication standards. This applies to the mobile handset antennas as well whose radiating dimensions are inversely proportional to the operating frequency. As the next generation Long Term Evolution (LTE) that supports lower frequency bands is deployed, the handset designers have to deal with the resulting larger antenna footprint and opt for the radiating topologies that function well in densely packed systems.

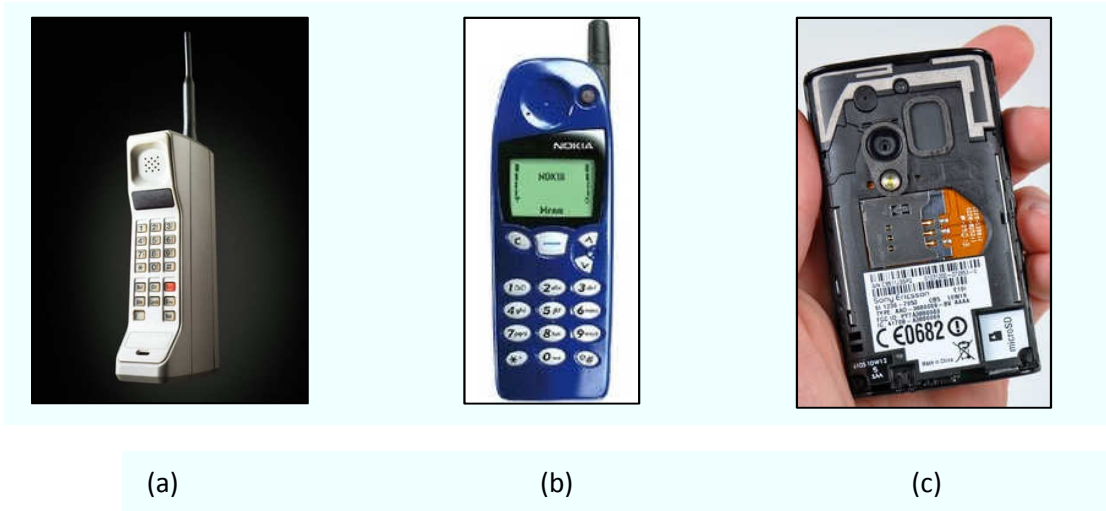


Fig. 1.1 (a) The Motorola DynaTAC with a monopole antenna. Image source: [1] (b) The Nokia 5510 with a helical antenna. Image source: [2] (c) The Sony Ericsson Xperia with the patch antennas visible at the top. Image source: [3]

The first commercially available cellular mobile handset was the Motorola DynaTAC in 1983 [4]. It used a monopole “whip” antenna operating in the 800 MHz frequency range which extended out of the main body of the handset, as shown in Figure 1.1(a). The monopole antenna provided an omnidirectional radiation pattern, which is ideal for a mobile handset. All of the mobile handsets in the 1980s featured monopole antennas. Research conducted on the monopole antennas concentrated on developing methods to control the radiation pattern [5, 6] and investigating the effect of users on the antenna performance [7].

In the mid-1990s, the monopoles were replaced by helical antennas, which were more compact. Figure 1.1 (b) shows the Nokia 5510, with a helical antenna.

When new telecommunication bands were introduced, such as GSM-1800, helical antennas were modified for multi-band operation [8, 9].

In the late 1990s, mobile handset manufacturers began to use patch antennas, which due to their low profiles and small footprints, could be integrated internally within the handset. This provided two advantages; a smaller handset size and the capability to design the antennas for directing less radiation towards the user's head [10, 11]. For these reasons, patch antennas became the most popular choice for cellular handset antennas in the first decade of the 21st century.

As additional telecommunication bands were introduced, such as GSM-1900 and GSM-2100, multi-band patch antennas were investigated [12, 13, 14, 15, 16]. To capture a growing and promising market, the functionality of the handsets was increased by incorporating additional systems, such as accelerometers and gyroscopes. This required for the patch antennas to have the smallest possible footprint and several methods were proposed to accomplish this goal [17, 18, 19]. Figure 1.1 (c) shows the Sony Ericsson Xperia, with the patch antennas integrated around the digital camera at the top of the phone. Other research on patch antennas focused on methods to increase the bandwidth [20, 21, 22] and to reduce the back radiation which is directed towards the user's head [23, 24].

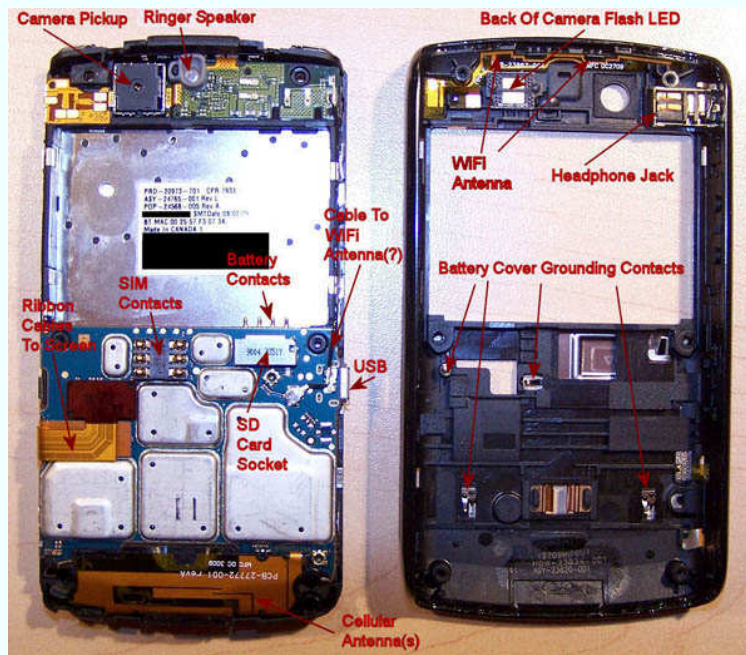


Fig. 1.2 The populated interior of the BlackBerry Storm. The LCD screen and battery have been removed to show the other on-board systems and antennas. Image source: [25]

The evolution of mobile handset antennas continues to this day. The increasing data requirements for modern mobile handsets have caused existing telecommunication frequency bands to become congested. To solve this problem, new bands and telecommunication protocols have been introduced such as the 3rd Generation Partnership Project (3GPP) Long Term Evolution (LTE) specification, which require handsets in North America to operate in the 700 MHz frequency range using multiple antennas [26]. It should be noted that LTE networks, when brought into commercial operation, have been marketed as 4th Generation (4G) networks as allowed by the International Telecommunication Union (ITU) [27].

Despite the extensive research conducted on patch antennas, they are not suitable candidates for LTE-compliant mobile handsets. The size of the patch antennas at the 700 MHz frequency band makes them difficult to place inside the congested volume of a typical handset, such as the one shown in Figure 1.2. Even if a suitable miniaturization technique is employed, such as the one proposed by the authors of [28] which can reduce the size of a patch antenna by up to 94%, a single patch antenna would still require a volume of 937.5 mm^3 (approximately) for the 700 MHz frequency range. With LTE specifications requiring multiple antennas being placed on the same handset, patch antennas remain too large to be practical.

Another type of antenna that is suitable for mobile handsets is the Printed Inverted-F Antenna (PIFA) [29]. The PIFA is a modified monopole and has a thin profile which allows for it to be placed next to components inside the handset. The PIFA is discussed in extensive detail in Section 1.2 and in Chapter 2.

It is apparent that future mobile handsets will require an alternative PCS antenna structure. The search for a suitable antenna structure poses several design challenges. To begin with, a suitable antenna for such future handsets will have to be small enough to fit inside the handset. In addition to size considerations, any antenna candidate must also take mutual coupling requirements into consideration. When multiple antennas are placed in close

proximity to one another, mutual coupling becomes an important performance-limiting factor because it degrades the antenna system's efficiency, gain and input impedance [30].

Mutual coupling between the antennas operating at different frequency bands poses as parasitic loading effects [31]. This is relevant for mobile handsets because they use several (separate) antennas for different wireless data services such as Wireless Local Area Networking (WLAN), Bluetooth and Global Positioning System (GPS). Each of these operates at different frequencies and their loading effects on one another must be taken into consideration. For multiple antennas operating at the same frequency band, such as LTE antennas, the mutual coupling is a more prominent problem resulting in channel co-relation, which deteriorates their data capacity [30].

1.2 Thesis Motivation

The work presented in this thesis is motivated by the need to investigate antenna structures that can operate within the limited available volume of a typical 4G mobile handset. It must be able to function at a level that is consistent with the operational requirements of a realistic mobile handset.

This thesis therefore investigates the suitability of the Printed Inverted-F Antenna (PIFA) as the antennas for a multi-antenna mobile handset. The PIFA is

a variant of the monopole [32, 33], where the main radiating arm has been folded to become parallel with the ground plane and a shorting arm has been added to obtain the desired input impedance. It provides good radiation characteristics and can be easily integrated with the other systems found in a handset. Furthermore, the thin profile allows for the PIFA to be mounted on the sides of the handset, thereby allowing the remaining device volume to be used more efficiently.

This thesis investigates the radiation characteristics of a two-antenna system of a semi-populated mobile handset. A semi-populated model is used to represent the handset and the antennas are PIFAs. Three different telecommunication bands, the LTE-Band 13 (746-786 MHz), the GSM-900 (890-960 MHz) and the GSM-1800 (1710 – 1880 MHz), are investigated and different sets of PIFAs are designed for each band while using the same semi-populated handset model.

Integrating multiple PIFAs that operate at the same frequency band within the confined volume of the handset poses several challenges. Since the performance of an antenna is highly dependent on its immediate environment, the first challenge is to design a suitable PIFA that takes into account the loading of other components found in a typical handset. The handset investigated in this thesis is therefore populated with two of the largest components that affect the

antenna performance found in every mobile handset – the battery and the LCD screen – and a design methodology for the antennas is presented.

Mutual coupling is a phenomenon that occurs in any multi-antenna system. This problem is further complicated when multiple antennas operate at the same frequency due to the significant increase in the mutual coupling. Before any reduction method can be suggested, it is important to investigate the mechanisms through which mutual coupling between the PCS antennas occur. The second objective of this thesis is therefore to present a profile of the antenna mutual coupling mechanism in the three telecommunication frequency bands for the handset.

The third and final objective of this thesis is to investigate mutual coupling reduction techniques. Various techniques have been reported to enhance isolation in multi-antenna systems [34, 35, 36, 37, 38, 39, 40]. With the lower frequency bands, the larger wavelengths of the signals make some of these techniques impractical for implementation in the small-form factor of the handset. This thesis explores mutual coupling reduction techniques that can be integrated in the limited volume of the handset and enhance isolation between the PCS antennas.

1.3 Thesis Contributions

In this thesis a comprehensive study of mutual coupling between the PIFAs of a 4G mobile handset at three telecommunication bands is presented. In particular, the first detailed investigation of a multi-PIFA structure below 1 GHz on a cellular mobile handset in the presence of other components is outlined in this dissertation. Moreover, various methods for enhancing antenna isolation are examined and the first design for antenna coupling reduction at the LTE Band-13 spectrum is introduced.

This thesis has resulted in the following conference publication so far:

1. **A. J. Wahidi**, S. M. Ali, R. Abhari “Investigation of Radiation Characteristics of a PIFA-Based Semi-Populated Handset Model for LTE B13”, Presented in the 2012 IEEE International Symposium on Antennas and Propagation, July 2012, Chicago

This paper which was selected as one of the *finalists in the student paper competition of the IEEE APS conference* discusses the design methodology and evaluation of handset PIFAs of the LTE-Band 13 handset. The contents of this paper are discussed in detail in Section 2.4.3 of the thesis.

For experimental validations, three printed circuit board prototypes are fabricated, tested and analyzed. The measurements obtained for the fabricated PCS LTE antennas of a semi-populated handset are being included in a journal paper that will be submitted to the IEEE Transactions on Antennas and Propagation.

1.4 Thesis Outline

This thesis begins with a description of a basic PIFA structure in Chapter 2. The parameters that control the different radiation characteristics of a PIFA are discussed and a design methodology is outlined. Using this design approach, a two-PIFA system is designed to work at the GSM-1800, GSM-900 and LTE-Band 13 spectrums. The results of the simulations and physical measurements are presented in Section 2.4.1, 2.4.2 and 2.4.3. A discussion on the why the PIFAs have different performance measurements at each frequency band is presented and the role of the ground plane in the radiation characteristics is highlighted.

The mutual coupling profiles for the three handsets are presented in Chapter 3. The dominant coupling paths are identified and are broadly categorized as being caused by either substrate-bound modes and/or space waves. A software simulation is then used to determine how the power between the two antennas is transferred at the three different frequencies.

Chapter 4 presents a brief survey of different mutual coupling reduction techniques presented in literature. The suitability of applying these methods to the mobile handset is discussed. The techniques deemed most feasible are then applied to the mobile handset at the three operating frequencies. The results are presented and the conclusions obtained from them are used to confirm the investigation carried out in Chapter 3.

Chapter 5 provides conclusions and suggestions for future work.

Chapter 2

Printed Inverted-F Antennas (PIFA) on a Semi-Populated Mobile Handset

2.1 Introduction

The Inverted-F Antenna has been studied extensively over the years. A theoretical model for the radiation resistance and input impedance for a wire Inverted-F Antenna was presented in 1960 using transmission line theory [41]. In the past decade, the Printed Inverted-F Antenna (PIFA) has been used extensively in wireless communication devices operating in the frequency bands for Wireless Local Area Network (WLAN) and Worldwide Interoperability for Microwave Access (WiMAX) (2.4, 3.4, 3.7 and 5 GHz) [42, 43, 32, 33]. The PIFA is well-suited for these applications because its physical size complies with the dimensions of the intended wireless devices. Besides, the antenna itself provides good gain and radiation efficiency. However, at lower frequencies, such as the telecommunication bands investigated in this thesis, the physical size of the PIFA is relatively larger and may not always be ideal for fitting on a handset. Fortunately miniaturization techniques such as meandering [29] or capacitive loading [44] can be employed to obtain an acceptably sized antenna.

This chapter begins by presenting the basic operational principle and design methodology of a PIFA in Section 2.2. Using the methodology outlined, Section 2.3 presents the PIFAs that are designed for the GSM-1800 (1710-1880 MHz), GSM-900 (890-960 MHz) and LTE-band 13 (746-786 MHz) spectrums. The radiation characteristics of the antennas designed for each band are then presented using software simulations and measurements of fabricated prototypes. All simulations presented in this thesis are conducted using Ansys/Ansoft HFSS Version 12, which is a commercially available Electromagnetic solver [45]. Section 2.4 presents the summary of this chapter.

2.2 Methodology to Design a PIFA

The Printed Inverted-F Antenna (PIFA) consists of a main radiating arm that is bent to become parallel with a ground plane. It also has a shorting arm that is added to control its input impedance [46], as shown in Figure 2.1.

The antenna has a complex input impedance which is a function of frequency. To match the antenna with a source with real impedance (often 50Ω), a shorting arm is added to the end of the radiating arm, which introduces additional inductive impedance.

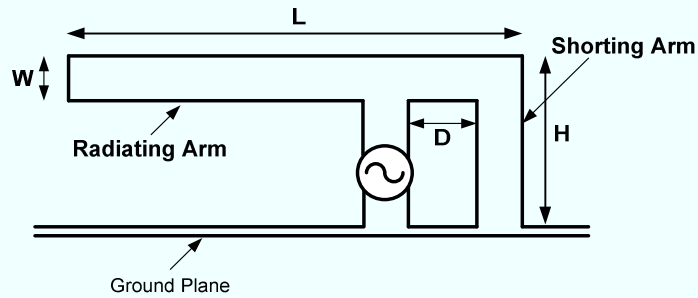


Fig. 2.1 The Printed Inverted-F Antenna. Length, L ; Height, H ; Radiating Arm width, W ; Distance between vertical Radiating Arm and Shorting Arm, D . Note: Thickness of Ground Plane is exaggerated for illustrative purposes.

The radiation characteristics of a PIFA can be controlled by varying the parameters that affect its resonance and input impedance. The length of the PIFA is inversely proportional to its resonance frequency. The relationship can be expressed by [47]:

$$f_r \sim \frac{c}{4(L+H)}, \quad \text{Eq. 2.1}$$

where f_r is the resonance frequency, c is the speed of light, L is the length of the PIFA and H is the height of the shorting arm. This relationship assumes that the PIFA is in a medium with relative permittivity of approximately 1 (i.e., free space). Equation 2.1 also reflects the similarity that a PIFA has with a monopole antenna. Like a monopole, a PIFA forms a radiating structure through the interaction of the main radiating arm with its image on the ground plane (resembling a dipole) [32]. For this reason, the ground plane plays an important role in the radiation characteristics of a PIFA.

Empirical data from simulations carried out in research works such as [32, 33] suggests that the optimum performance can be achieved when the ground plane is at least $\lambda/4$ in length in the direction of the dominant current distribution on the ground plane.

An attractive feature of a PIFA is the ability to control the imaginary component of its input impedance by changing its layout parameters. Specifically, the distance, D , between the shorting arm and the vertical portion of the radiating arm can be used to control the reactive impedance of the antenna. The value of the reactive impedance is inversely proportional to the value of D [32]. By varying the distance D , the reactive impedance may be canceled, resulting in a real input impedance.

The width W of the main radiating arm of the PIFA is the second parameter that controls different characteristics of the antenna. The first characteristic is the reactive impedance. Increasing the width W of the antenna arm brings it closer to the ground plane (for fixed H) thereby creating a higher capacitance. Another characteristic is the bandwidth, which is directly proportional to the value of W . Increasing the width of the radiating arm extends the operating bandwidth [32].

The final characteristic affected by the width is the resonance frequency. Alternatively, if the resonance frequency of the antenna must be kept constant, the width allows for the length, L , to be changed. This fact can be utilized to

miniaturize the antenna length. For example, if the width is increased, the length of the antenna can be reduced.

To design a PIFA for a given resonance frequency, the first step to consider is the constraints on the height or length of the structure. For example, the handset investigated in this thesis cannot accommodate an antenna that has a height greater than that of the handset itself. Once such restraints are factored in, Equation 2.1 may be used to determine a starting point for the length L and the height H of the PIFA. An iterative design process may be required to obtain the correct combination. Once the resonance frequency is obtained, the value of D can be varied in order to obtain the desired input impedance. This generally causes a slight shift in resonance frequency, requiring the length or height to be readjusted [33]. If the PIFA does not satisfy bandwidth requirements, the parameter W can be increased. This may once again cause the resonance frequency to shift but can be corrected by varying the length of the antenna[33].

This iterative process may require several rounds before a final design provides acceptable results. The use of optimization procedures in software simulation tools simplifies this task considerably.

2.3 The Design and Analysis of a PIFA for a Mobile Handset Form Factor

In order to ensure a successful PIFA design a realistic model for the cellular mobile handset should be used in simulations. The mobile handset structure considered in this thesis is based on a “smartphone”, a moniker given to mobile handsets with increased functionality. The mobile handset is 95 mm in length and 60 mm in width. The other dimensions for the handset box are shown in Figure 2.2(a). The handset is modeled by a hollow box and in developing the test prototype it is constructed by six pieces of FR4 substrate that are glued together to form the handset box. FR4 is a readily available epoxy based laminate [48] - the FR4 substrate used has a relative permittivity of 4.4, dielectric loss tangent of 0.02 and thickness of 1.5 mm. The simulated handset models represent the prototypes that are commonly built for design evaluations at Research In Motion Limited (RIM), Canada, before adoption of the structure for mass production.

To study the interaction of the PIFAs with the components found in a handset, models of a battery and an LCD screen have been added, which are two of the largest handset parts. The battery is represented by a box of dimensions 51 mm X 40 mm X 6 mm. The box is constructed of copper sheets with 35 μm thickness. The LCD screen is 32 mm X 45 mm copper sheet (35 μm thick).

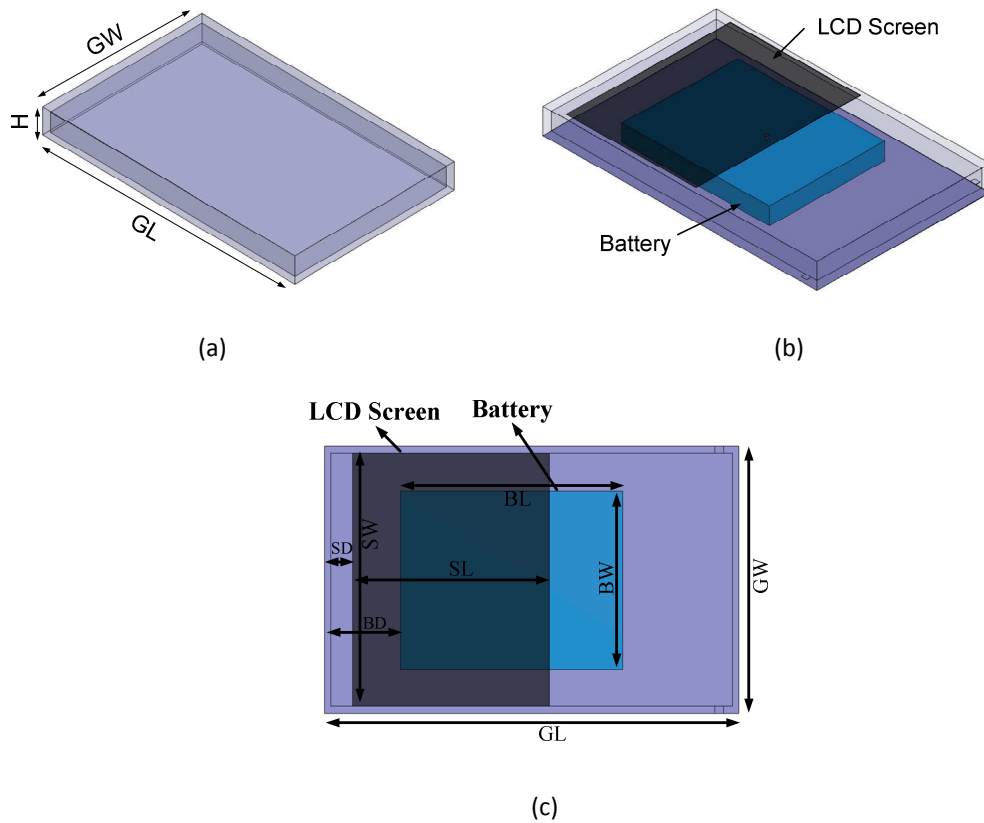


Fig. 2.2 The investigated handset (without the antennas) (a) The 3D view of the unpopulated handset. (b) The 3D view of the semi-populated handset (c) Top view with labeled parameters of the semi-populated handset.

Dimensions: $GW=60$, $GL=95$, $H=9$, $BW=40$, $BL=51$, $SW=45$, $SL=32$, $SD=6.5$, $BD=17.5$

(all values in mm)

The battery and LCD screen are both grounded using solid copper vias with a radius of 0.478 mm at the center of the mobile handset.

The antennas are modeled by copper sheets that are 35 μm thick. Figure 2.2(b) depicts the 3D semi-populated handset model. The layout of the components on the semi-populated handset is shown in Figure 2.2(c).

The antennas presented in this chapter are deemed for operation at the LTE-Band 13, GSM-900 and GSM-1800 telecommunication bands. The antennas are designed to satisfy certain operating criteria used by Research In Motion (RIM). These performance targets are outlined in Table 2.1. It may be noted that the performance criteria for the LTE-Band 13 spectrum is not as stringent as the other two spectrums. This is because the size of the antennas at the 750 MHz frequency range becomes too large for the considered form factor to reasonably expect good performance levels.

In the handset models considered in the following sections and throughout this thesis, a two-antenna structure is always developed. This is due to the increasing data requirements for future handsets. Handset users generally receive more data than they transmit and the antennas are therefore designed so that one of them can transmit but both can receive. This enables the bandwidth of the downlink to be larger than the uplink and allows users to utilize higher data-rate services, such as video streaming.

Table 2.1 Performance Requirements for the Mobile Handset Antennas.

Characteristic	Frequency Band	Required
Reflection Coefficient	LTE-Band 13	< -5 dB
	GSM-900	< -5 dB
	GSM-1800	< -10 dB
Mutual Coupling	LTE-Band 13	< -10 dB
	GSM-900	< -15 dB
	GSM-1800	< -15 dB
Antenna Efficiency	LTE-Band 13	> 25%
	GSM-900	> 45%
	GSM-1800	> 65%

2.3.1 PIFA Design for GSM-1800

The highest frequency band investigated in this thesis is the GSM-1800 spectrum, which was introduced commercially in 1992 [49] and is now used throughout the world. The GSM-1800 spectrum extends from 1710 MHz to 1880 MHz and is split into two 75 MHz bands. The uplink band extends from 1710 MHz to 1785 MHz. The downlink band extends from 1805 MHz to 1880 MHz.

Considering the two-antenna handset, the PIFAs for the mobile handset are designed in a two step process using the design methodology outlined in section 2.2. In the first step, the PIFAs are designed to operate on an unpopulated handset, such as the one depicted in Figure 2.2(a). In the second step, the components are added to the handset and the antennas are re-tuned in order to satisfy the performance targets.

Using the methodology previously presented, the design process begins by placing both PIFAs on the unpopulated handset. The two antennas are positioned on the side walls of the handset starting from the lower end, as shown in Figure 2.3(a). The height of the PIFAs is restricted by the thickness of the handset and is therefore set to 9 mm. The width of all the parts of the antenna is set to 2 mm initially and the length of the antenna is varied until a resonance frequency is achieved in the middle of the GSM-1800 band (1795 MHz). The

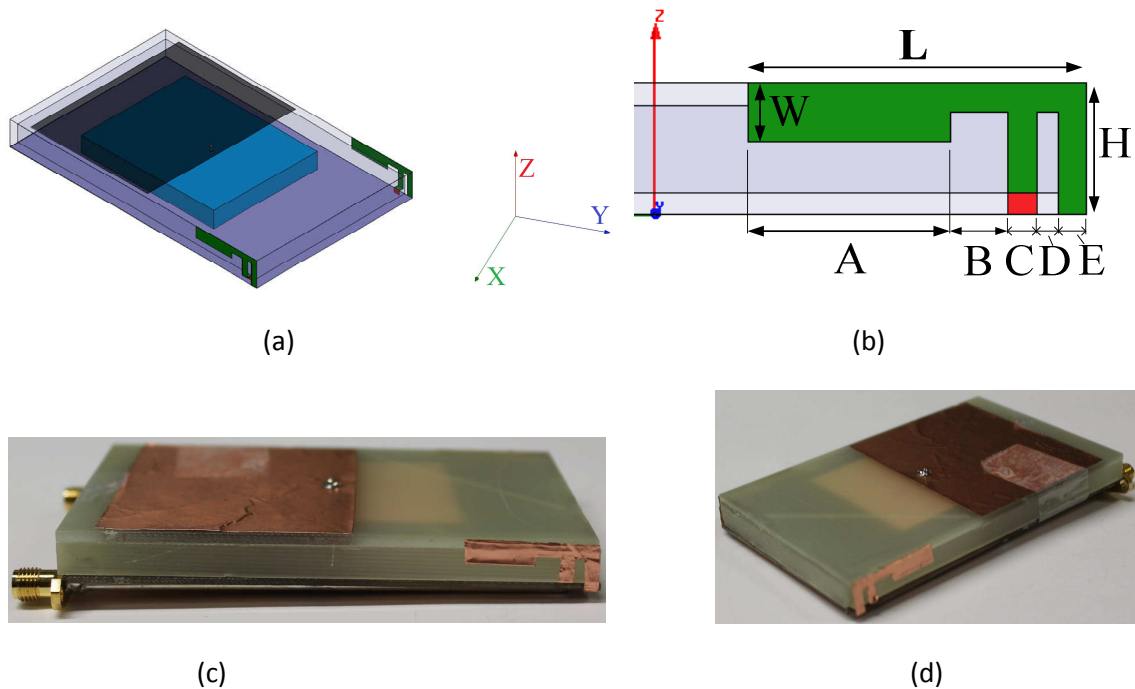


Fig. 2.3 The GSM-1800 Handset (a) Positioning of the PIFAs on the handset (b) The designed PIFA for GSM-1800 MHz (c) Side view of the Antenna #1 on the fabricated handset (d) 3D view of Antenna#2 on the fabricated GSM-1800 handset.

Dimensions: $L=23.5$, $W=4$, $H=9$, $A=13.9$, $B=4$, $C=2$, $D=1.5$, $E=2$ (all units are mm)

sum of the length and the height (9 mm) for both of the initial PIFAs is 35.5 mm which is 15% shorter than a quarter-wavelength ($\lambda/4=41.6$ mm) at 1800 MHz.

After placing the antennas on a semi-populated board in the second step, the interaction of the antennas with the components causes the center of the resonance frequency of both PIFAs to shift from 1795 MHz to 1750 MHz. This also results in the antenna bandwidth reduction for both of them from 219 MHz for the unpopulated board to 166 MHz for the semi-populated board.

In order to increase the bandwidth and to retune the antennas to operate at the correct frequency band, the width of the antenna arm for both PIFAs is increased from 2 mm to 4 mm. This increases the bandwidth of both antennas and allows for the size (i.e., L+H) for both the antennas to be reduced from 35.5 mm to 32.5 mm (a reduction of 8.4%). The final version of the PIFA design is presented in Figure 2.3(b). The feeding point for the antenna is at the bottom of the vertical arm parallel to the shorting arm and is modeled as a lumped port in the HFSS simulations. This version was fabricated and the simulated and physical measurements are presented in Table 2.2.

2.3.1.1 Simulation Results

The simulation results from HFSS show that the PIFAs operate efficiently at the GSM-1800 band. One reason for this is that at this frequency, the ground plane is $0.36\lambda \times 0.57\lambda$ and is therefore large enough to support a full resonant current distribution.

The reflection coefficient is the same for both antennas and remains below the -10 dB level as required, as seen in Figure 2.4(a). The bandwidth of both antennas is 186 MHz which is wide enough to allow for both antennas to cover both the uplink and downlink bands. The PIFAs achieve a relatively high gain, as

shown in Figure 2.5 (a) and (c). The radiation patterns are generated for the $\Phi = 0$ plane only for brevity.

The mutual coupling between the antennas however is higher than the design limits allow. An investigation is carried out in Chapter 3 to determine the cause of this and methods to reduce the coupling are investigated in Chapter 4.

2.3.1.2 Measurement Results

The GSM-1800 handset antennas modeled in the final simulations were fabricated at the RIM facilities in Waterloo, Canada. Figure 2.3(c) and Figure 2.3(d) show pictures of the developed models.

The measurements of the test structures, provided in Table 2.2, confirm that the model adheres to the design guidelines and follows the trend shown in the simulations. Figure 2.4(b) shows the reflection coefficients and mutual coupling between the antennas. The reflection coefficients for both antennas are identical, as predicted, and are centered around 1805 MHz (as opposed to 1795 MHz in the simulations). The mutual coupling was observed to be 2 dB higher than the simulations.

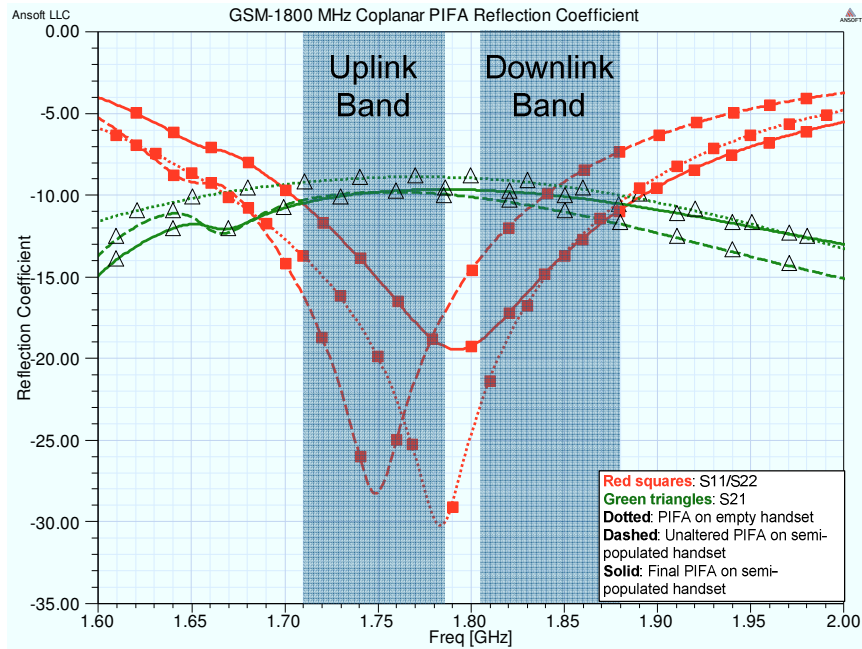
The radiation efficiency measured for both antennas are lower than those predicted by simulations but meet the operating target. Figure 2.5(b) and Figure 2.5(d) show the measured radiation patterns for each antenna. It can be seen

that Antenna #1 and Antenna #2 both achieve gains that are slightly lower than the simulated values. Both gains however are at acceptable levels.

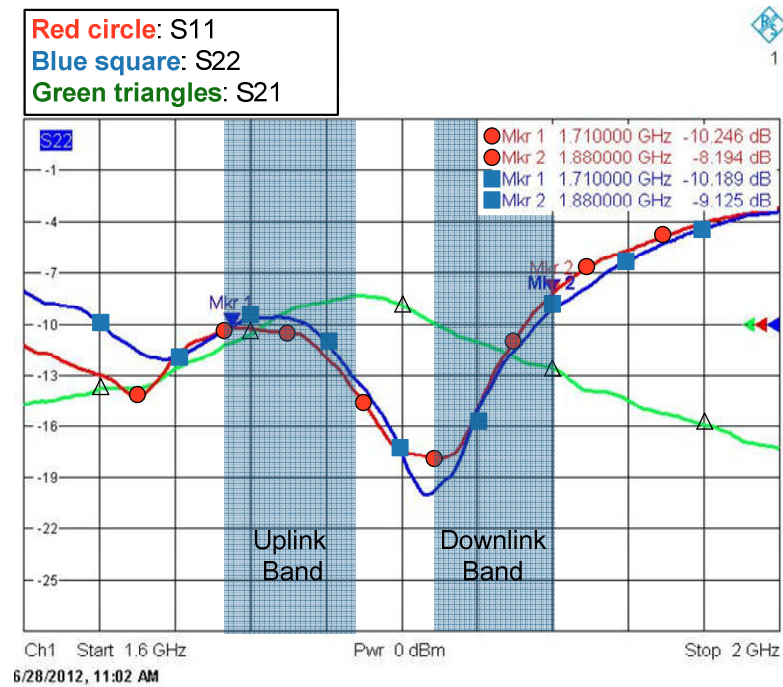
The differences between measured and simulated results are attributed to the non-ideal prototypes used for measurements: It can be seen from the pictures that semi-rigid coaxial cables are used to feed the antennas and tapes are used for mounting them on the boards. In constructing the metal parts, copper tapes and sheets are used and the effects of glue layer underneath them and in between the FR4 boards constructing the handset model are not included in the simulations.

Table 2.2 Simulated and Measured Performance of Antennas for GSM-1800 Handset.

Characteristic	Simulated Values (dB)	Measured Values (dB)
Reflection Coefficient in Uplink band	-19.5 < S_{11} < -11.6 -17.9 < S_{22} < -10.4	-13.9 < S_{11} < -10.1 -14.1 < S_{22} < -10
Reflection Coefficient in Downlink band	-19.5 < S_{11} < -11.6 -17.9 < S_{22} < -10.4	-19.5 < S_{11} < -11.6 -17.9 < S_{22} < -10.4
Mutual Coupling in Uplink Band	-10.1 < S_{21} < -9.55	-18.7 < S_{21} < -11.2
Mutual Coupling in Downlink Band	-10.5 < S_{21} < -9.62	-18.7 < S_{21} < -11.2
Maximum Gain Antenna #1	4.3	2.98
Maximum Gain Antenna #2	4.26	3.18
Antenna #1 Radiation Efficiency	80.2%	58%
Antenna #2 Radiation Efficiency	79.9%	62%



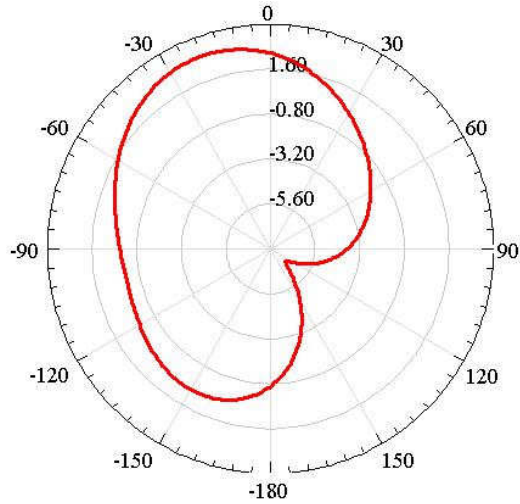
(a)



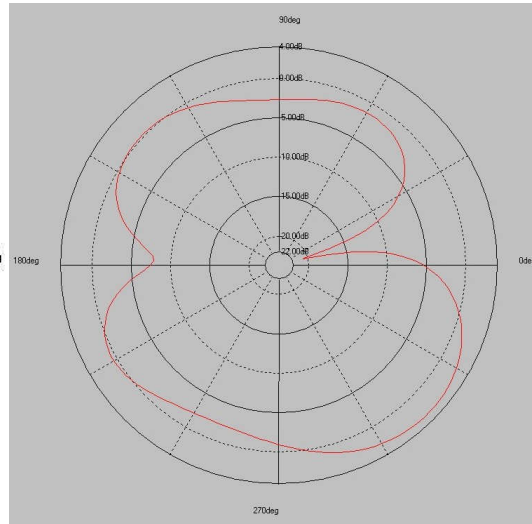
(b)

Fig. 2.4 The S-Parameter for the Antennas of the GSM-1800 Handset (a) Simulation results

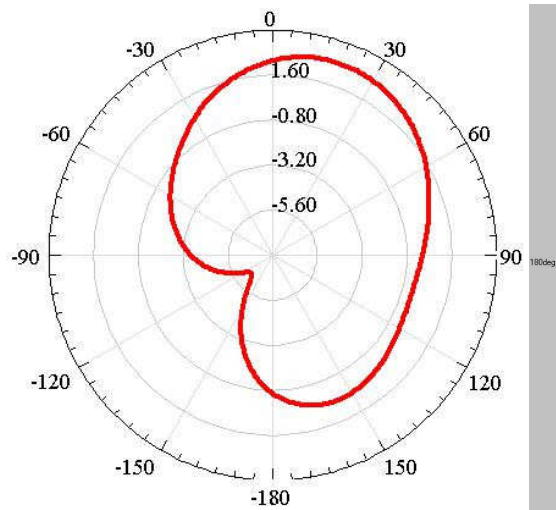
(b) Measurement results.



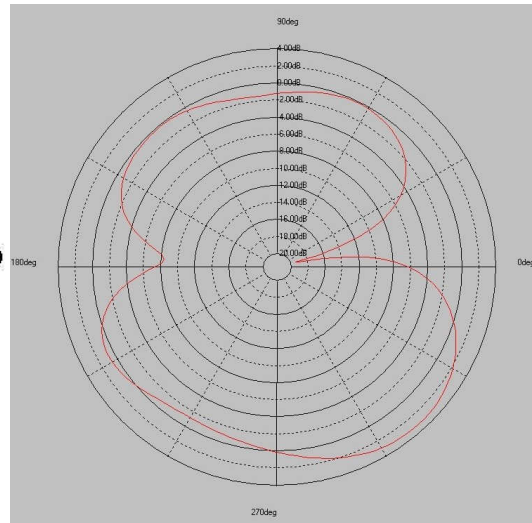
(a)



(b)



(c)



(d)

Fig. 2.5 The Radiation Pattern for the semi-populated GSM-1800 handset at 1.8 GHz ($\varphi = 0$) (a) Simulation result for Antenna #1 (b) Fabricated result for Antenna #1 (c) Simulation result for Antenna #2 (d) Fabricated result for Antenna #2.

2.3.2 PIFA Design for GSM-900

The GSM-900 band was the first frequency band in the GSM spectrum that was made commercially available in 1990 [49]. The GSM-900 band extends from 890 MHz to 960 MHz and is split into an uplink band (890-915 MHz) and a downlink band (925-960 MHz).

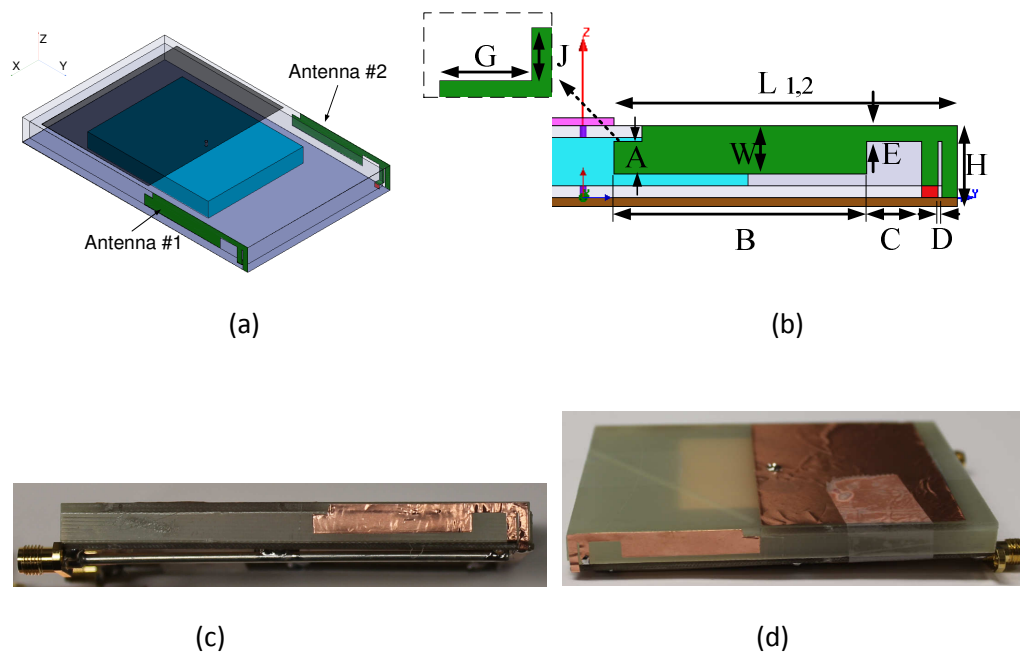


Fig. 2.6 The GSM-900 Handset (a) Positioning of the PIFAs on the Handset (b) The Designed PIFA for the GSM-900 Handset (c) Side view of Antenna #1 on the fabricated handset (d) 3D view of Antenna #2 on the fabricated handset.

Dimensions: $L_1=37.8$, $L_2=40$, $W=6$, $H=9$, $A=4$, $B=32$, $C=7$, $D=0.5$, $E=2$; $G=3.5$, $J=2$ (All units are mm)

The performance targets for the GSM-900 band are almost identical to those of the GSM-1800 band, with the exception of the reflection coefficient. This is lower for the GSM-900 band due to the smaller electrical size of the ground plane ($0.19\lambda \times 0.29\lambda$) at the 900 MHz frequency range.

The design process for the GSM-900 handset repeats the two-step process used for the GSM-1800 handset in Section 2.3.1. In the first step, the antennas are designed on an unpopulated handset and in the second step the components are added to the handset and the antennas are retuned.

The design starts by placing Antenna #1 and Antenna #2 on the unpopulated board. The PIFAs are positioned once again towards the bottom of the handset, as shown in Figure 2.6(a). Both antennas are 9 mm in height and all the arm widths on both antennas are initially set to 2 mm. After conducting a parameter sweep on the length of both antennas, it was found that the bandwidth for the PIFAs is no longer large enough to cover both the uplink and downlink bands simultaneously. Fortunately, the GSM specifications do not require for multiple antennas [50]. Antenna #1 is therefore designed to operate in the uplink band only while Antenna #2 is designed to operate in the downlink band only. The size of Antenna #1 (i.e., L+H) is found to be 60.7 mm which is 73% of the quarter-wavelength ($\lambda/4=83.1$ mm) at 902.5 MHz, i.e., the center of the uplink

band. The size of Antenna #2 is 57.7 mm which is 72.8% of the quarter-wavelength at 947.5 MHz ($\lambda/4=79.1$ mm), i.e., the center of the downlink band.

The two PIFAs are then added to a semi-populated board without altering their size. The resonance frequency of Antenna #1 is noted to shift from 902 MHz to 771 MHz while the resonance frequency of Antenna #2 shifts from 947 MHz to 840 MHz. The bandwidth of Antenna #1 also decreases from 71 MHz to 36 MHz while the bandwidth of Antenna #2 drops from 83 MHz to 49 MHz.

The main reason for this large degradation is the close proximity of the components, in particular the LCD screen to the antennas. The LCD screen acts like a loading parasitic plane which is grounded. Any current distribution on the antennas especially near the LCD screen creates a current distribution (dominantly in the opposite direction) on the LCD screen. This interaction of currents creates a capacitive loading for the antennas and therefore lowers their resonance frequencies.

Since the presence of the components prevents the antennas from achieving their maximum performance levels, it is important to miniaturize the footprint of the antennas to the extent possible. The width of the arms in both antennas is therefore increased from 2 mm to 6 mm, to allow the length of the antenna to be decreased. The total size of Antenna #1 in the final design is 46.8 mm (22.8% reduction) whereas the total size of Antenna #2 is 49 mm (15% reduction).

Despite the reduction in length, the end of each antenna remains in close physical proximity to the LCD screen. To further increase the isolation, a rectangular section is cut from the top end of each radiating arm. The size of this chipped portion is varied until the antennas operate within the desired performance levels.

Widening the radiating arm also increases the reactive part of the antenna's input impedance. In order to maintain a real input impedance, the reactive impedance has to be decreased and distance D is therefore reduced. The final design of the PIFA for the GSM-900 band is shown in Figure 2.6(b).

This design is simulated in HFSS and is used as the basis for the fabricated model. The simulated and measured results are summarized in Table 2.3.

2.3.2.1 Simulation Results

The simulations show that the increase in antenna arm width and the introduction of the chipped portion allows for the antennas to cover their respective bands, as shown in Figure 2.7(a).

The simulations indicate that the GSM-900 PIFAs experience a considerable drop in performance in comparison to the PIFAs designed for the GSM-1800 band. This is expected, as noted earlier, due to the smaller size of the ground plane which results in dropping the maximum gain to 0.36 dB for Antenna #1 and

to -0.02 dB for Antenna #2. The radiation patterns for the individual antennas are shown in Figure 2.8(a) and Figure 2.8(c).

Once again it should be noted that the mutual coupling for the GSM-900 handset is slightly higher in the downlink band than what is allowed by the performance targets. The cause for this is investigated in Chapter 3 and methods to reduce it are presented in Chapter 4.

2.3.2.2 Measurement Results

The fabricated model for the GSM-900 handset is shown in Figure 2.6(c) and Figure 2.6(d). The measurement results are listed in Table 2.3. The reflection coefficients and mutual coupling are presented in Figure 2.7(b). The results show that Antenna #1 performs better than the simulated model, exhibiting a sharper resonance. The measurements of Antenna #2 however show some discrepancies although it is meeting the operational targets. The deviation in the performance of Antenna #2 is attributed to fabrication errors. Antenna #2 demonstrates a larger bandwidth and a sharper resonance than the simulated model. The measured values are higher than the predicted values.

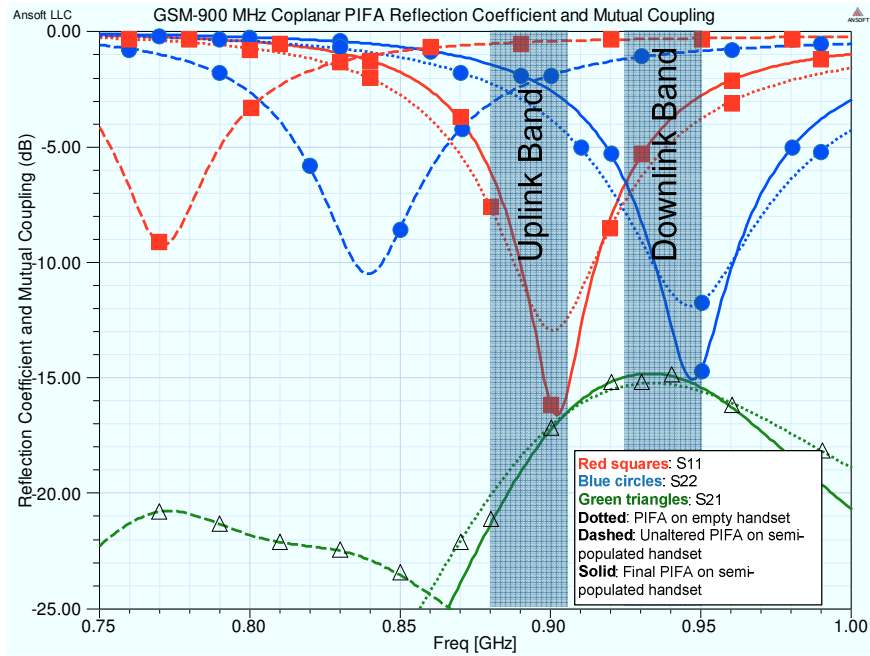
The measured radiation patterns measured of each antenna are shown in Figure 2.8(b) and Figure 2.8(d). Once again, only the radiation pattern for $\Phi=0$ is shown for purposes of brevity. Antenna #1 delivered a gain of -0.02 dB while

Antenna #2 has a gain of -3 dB. The radiation efficiencies of both antennas are lower than their respective simulated counterparts while still reaching the operational targets.

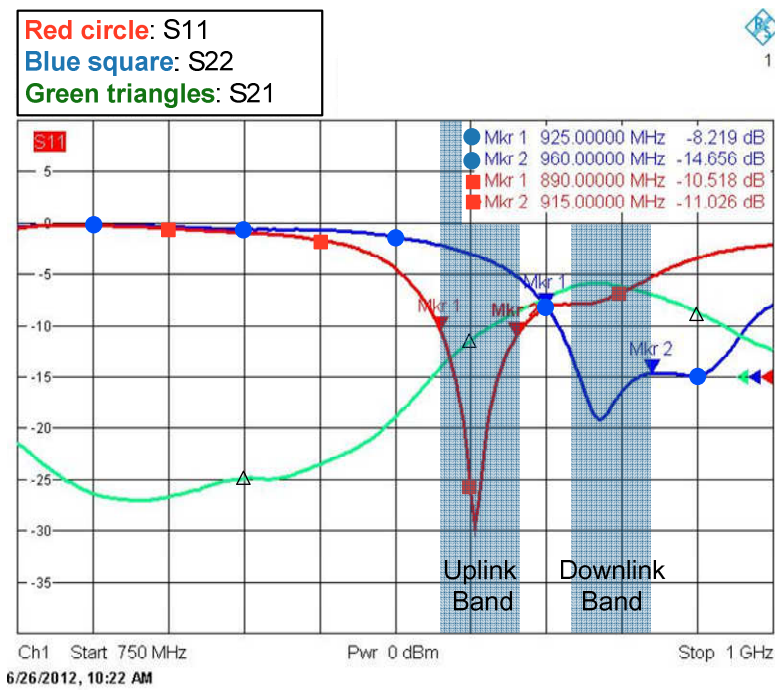
The differences between measured and simulated results are attributed to non-ideal fabrication method of the prototypes as discussed at the end of Section 2.3.1.2.

Table 2.3 Simulated and Measured Performance of GSM-900 Handset Antennas.

Characteristic	Simulated Values (dB)	Measured Values (dB)
Reflection Coefficient in Uplink band	$-16 < S_{11} < -6$	$-31 < S_{11} < -10.5$
Reflection Coefficient in Downlink band	$-15.9 < S_{22} < -6$	$-18.5 < S_{22} < -14.6$
Mutual Coupling in Uplink Band	$-19.1 < S_{21} < -15.5$	$-14.5 < S_{21} < -8$
Mutual Coupling in Downlink Band	$-16 < S_{21} < -14.7$	$-7 < S_{21} < -5.5$
Maximum Gain Antenna #1	0.36	-0.02
Maximum Gain Antenna #2	-0.02	-3
Antenna #1 Radiation Efficiency	67.7%	48%
Antenna #2 Radiation Efficiency	69.9%	28%

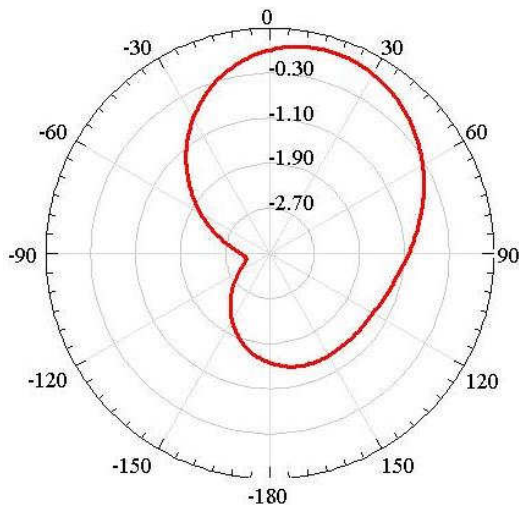


(a)

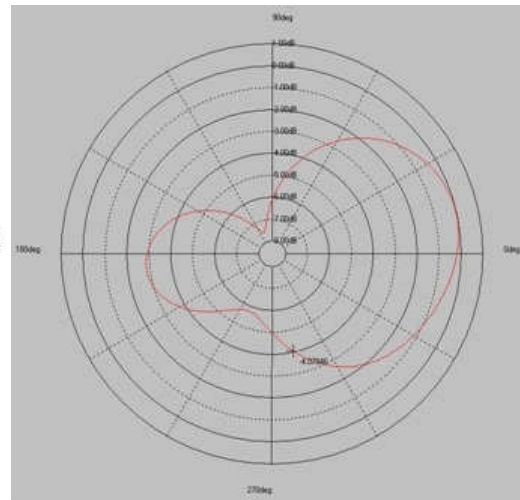


(b)

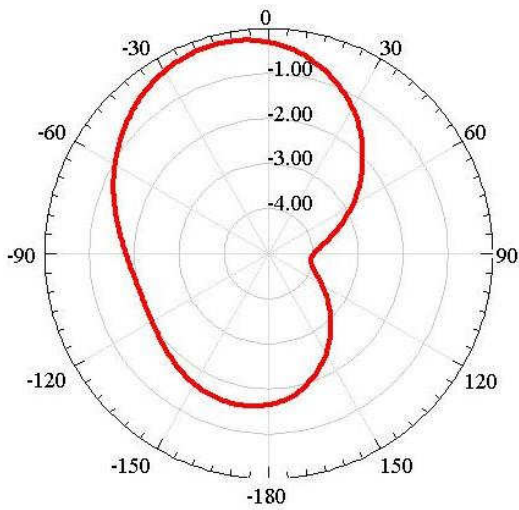
Fig. 2.7 The S-Parameter for the Antennas of the GSM-900 Handset (a) Simulation results (b) Measurement results.



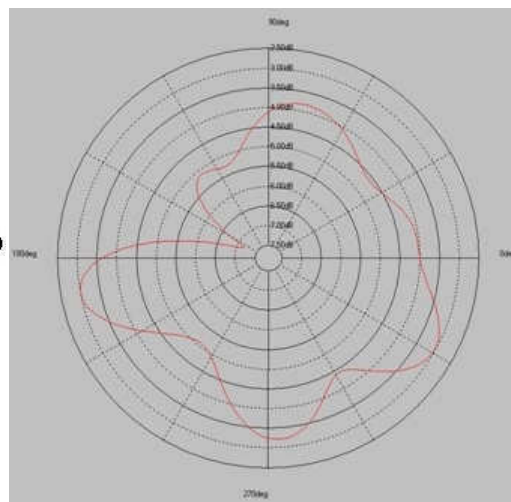
(a)



(b)



(b)



(d)

Fig. 2.8 The Radiation Pattern of the semi-populated GSM-900 handset antennas at 925MHz ($\varphi=0$) (a) Simulation result for Antenna #1 (b) Measured result for Antenna #1 (c) Simulation result for Antenna #2 (d) Measured result for Antenna #2.

2.3.3 PIFA for LTE-Band 13

The exponential increase in mobile handset users in the past decade has placed a severe strain on the existing telecommunication spectra. The popularity of video streaming has further exasperated the situation. To alleviate the problem, new spectral bands are being introduced to enable faster and more reliable service [51]. The introduction of the LTE standard is part of this strategy.

This thesis focuses on the lower LTE spectrum, in particular the LTE Band 13. The LTE Band-13 extends from 746 MHz to 786 MHz and consists of a downlink (746-756 MHz) and an uplink band (776-786 MHz).

It is interesting to note that unlike the GSM bands, the uplink band for the LTE-Band 13 is allocated to the higher frequency band. One reason for this may be to provide as much frequency isolation as possible for the uplink band from the 600 MHz spectrum at which broadcast television stations currently operate (as of 2012). The high power transmitted signals from these stations would overpower the relatively weak uplink signal of a mobile handset in the detection process. The uplink is therefore allocated to the higher frequency band to ensure a robust connection. The telecommunication network has the infrastructure to transmit a downlink signal with sufficient power to be detected.

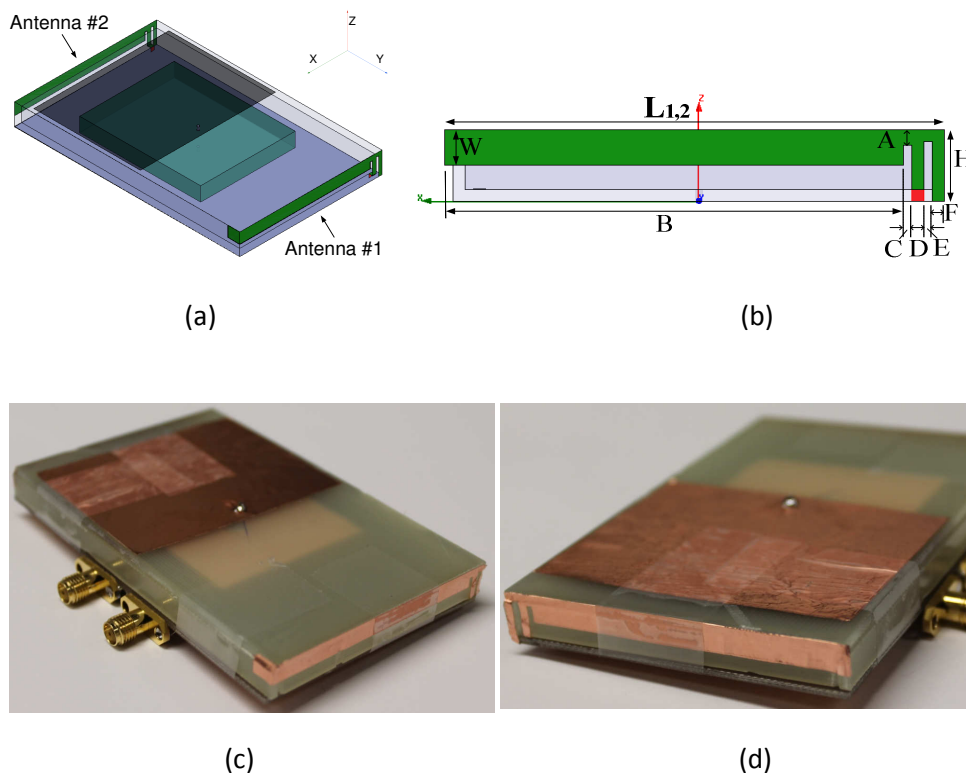


Fig. 2.9 The LTE-Band 13 Handset (a) Positioning of the PIFAs on the handset (b) The Designed PIFA for the LTE Band 13 Handset (c) 3D view of the fabricated model showing (c) Antenna#1 and (d) Antenna #2.

Dimensions: $L_1=65$, $L_2=60$, $W=4.5$, $H=9$, $A=2$, $B=55$, $C=1$, $D=1.5$, $E=1.5$; $F=1.5$ (all units

Using Equation 2.1, the length of the PIFA for the LTE-Band 13 spectrum is calculated to be approximately 90 mm. If the two PIFAs are placed at the longer sides of the handset, as was done for the GSM handsets, the larger arm of both would be close to the LCD and battery. In the design of the GSM-900 handset, these components were noted to deteriorate the performance of the antennas. The conducted parametric simulations in this research work demonstrated that

the application of a miniaturization technique such as meandering and folding would not result in well-performing LTE PIFAs while maintaining sufficient physical separation from other components. Therefore, the antennas must be re-positioned.

An investigation, not presented here, was carried out to determine the best positions for the LTE-Band 13 PIFAs. It was concluded that placing the antennas on the top and bottom of the handset, as shown in Figure 2.9(a), provides the best overall results. An advantage to this layout is that one of the antennas is farther from the two large components and can radiate with better efficiency. In addition to this, the ground plane stretches along its longer side (0.24λ) between the antennas, which is close to the length required for optimum ground plane performance [32].

The design repeats the two-step process used earlier. The LTE-Band 13 PIFAs are first designed considering an empty handset. The initial size of Antenna #1 and Antenna #2 (i.e., L+H) is 80.4 mm which is 82.1% of a quarter-wavelength at the center frequency of the LTE-Band 13 ($\lambda/4=97.9$ mm at 766 MHz).

The PIFAs are then simulated when placed on a semi-populated handset. As expected, a shift in the resonance frequency is noted for both antennas, from 766 MHz to 756 MHz for Antenna #1 and a larger shift from 766 MHz to 718 MHz

for Antenna #2 which is due to being closer to the LCD screen. The bandwidths (bandwidth for LTE-700 defined as $S_{11} < -5$ dB) also reduce from 48 MHz to 32 MHz for Antenna #1 and from 48 MHz to 25 MHz for Antenna #2.

Next the final antenna layouts are optimized via fullwave simulations to increase the bandwidth and to bring the resonance frequency within the LTE Band 13 spectrum.

The width of the radiating arm of both antennas is first increased from 2 mm to 4.5 mm. This allows the length of the radiating arm of Antenna #1 to be reduced to 74 mm (i.e., a 7.9% reduction). Since this length is too long to fit completely on the bottom side of the handset, a part of its radiating arm is wrapped around the corner and extended to the perpendicular wall. Increasing the width of the radiating arm of Antenna #2 reduces its length to 69 mm (i.e., a 14.1% reduction). Antenna #2 experiences an extra capacitive loading due to its proximity to the LCD screen which results in further reduction of its length in comparison with Antenna #1. The final designs for the LTE-Band 13 PIFAs are presented in Figure 2.9(b).

These layouts are further simulated in three different excitation scenarios. Since the LTE specifications require the handsets to operate with multiple antennas, each antenna is expected to perform efficiently in singly-fed mode, as well as together with the other antenna. In the first scenario, both antennas are

excited. In the second scenario, Antenna #1 is excited while Antenna #2 is terminated to a matched load. In the third scenario, Antenna #2 is excited while Antenna #1 is terminated to a matched load.

2.3.3.1 Simulation Results

The results for the simulation are provided in Table 2.4. The designed PIFAs cover both the uplink and downlink bands, as required. The reflection coefficients and mutual coupling for the simulations are plotted in Figure 2.10(a). The bandwidth (defined as $S_{11/22} < -5$ dB) for Antenna #1 is 54 MHz and 47 MHz for Antenna #2. Both antennas remain below the -5 dB operational target in both bands. The mutual coupling however is above the -10 dB threshold. Chapter 4 presents a mutual coupling reduction method to bring the coupling level below acceptable limits.

An interesting observation here is that the radiation pattern, gain and efficiency depend on the phase difference between the excitations of the two antennas. Table 2.5 summarizes the differences in performance of the two antennas when they are excited by 0, $\pi/2$ and π radians phase difference. Figure 2.11 shows that the radiation pattern varies with changing the feeding phase difference. The reflection coefficients and mutual coupling do not change noticeably in their frequency domain signatures.

Subsequent simulations explained that the change in radiation patterns of the two antenna system is due to the different current distributions on the ground plane at various excitation scenarios. The ground plane, at the LTE-Band 13 frequency, is $0.15\lambda \times 0.24\lambda$. When the antennas are placed at the top and bottom of the handset, they are separated by 0.24λ . This is close to the optimum size of the ground plane for a single antenna [32]. This also happens to be the side of the ground plane that contributes most to the radiation. However, with two antennas sharing the same ground plane, the interactions of the current distributions set up by each antenna become a determining factor in the overall performance of the system.

When the phase difference between the two antennas is zero, the currents from both antennas are in the opposite directions, canceling each other's effect. This is shown in Figure 2.12(a). On the other hand, when the phase difference is set to π , the current distributions are in the same direction, as shown in Figure 2.12(b), allowing the ground plane to contribute to the radiation. For a phase difference of $\pi/2$, the current distributions do not completely add or subtract from one another, resulting in a radiation efficiency that lies between the two extremes. In this thesis, the case where both antennas are connected to an excitation source (whether they are in phase, out of phase or phased by a $\pi/2$ difference) is referred to as the first scenario.

In the second scenario, where Antenna #1 is excited while Antenna #2 is terminated to a matched load, the radiation pattern, presented in Figure 2.13(a) shows that wrapping the antenna around the bottom corner of the handset does not alter its shape. The radiation efficiency and gain for Antenna #1 are listed in Table 2.6.

In the third scenario, Antenna #2 is excited while Antenna #1 is terminated to a matched load. The radiation pattern of Antenna #2, shown in Figure 2.13(c), is similar to that of Antenna #1 except for the gain and efficiency, listed in Table 2.7, that are much lower. The suboptimal performance here is due to the closeness of the LCD screen as explained earlier.

2.3.3.2 Measurement Results

The fabrication and measurements of the LTE-B13 handset prototype were conducted at the RIM facilities in Waterloo, Canada. Pictures of the constructed model are shown in Figure 2.9(c) and Figure 2.9(d).

The measured reflection coefficient and mutual coupling, presented in Figure 2.11(b), show that Antenna #1 exhibits a sharper resonance than its simulated counterpart. The resonance of Antenna #2 on the other hand is shifted from 1.76 GHz in the simulations to 1.82 GHz in measurement. This may be attributed to the additional parasitic loading effects of the soldering and feeding wires in the

fabricated model. Due to the displacement of the resonance frequency of Antenna #2, the measured S21 between the antennas is lower than the simulated results.

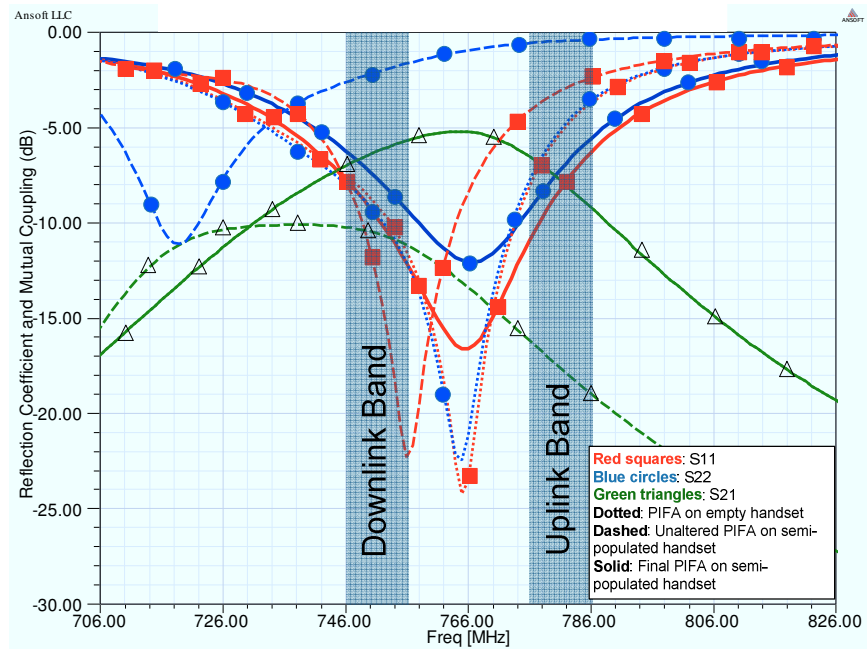
The anechoic chamber used for the radiation pattern and radiation efficiency measurements had only one port available. Therefore only the second and third source connection scenarios were tested. In the second scenario, the $\Phi=0$ cut plane of the radiation pattern of Antenna #1, shown in Figure 2.13(b), depicts a similar profile as the simulations. The measured gain, listed in Table 2.6, is slightly higher. In the third scenario, the $\Phi=0$ cut-plane of the radiation pattern of Antenna #2, shown in Figure 2.13(d), showed little similarity to the simulation results due to the shift in the resonance frequency and other possible measurement errors. The gain and efficiency of Antenna #2, listed in Table 2.7, are also lower for the same reason.

Table 2.4 Simulated and Measured Performance of LTE-B13 Handset Antennas.

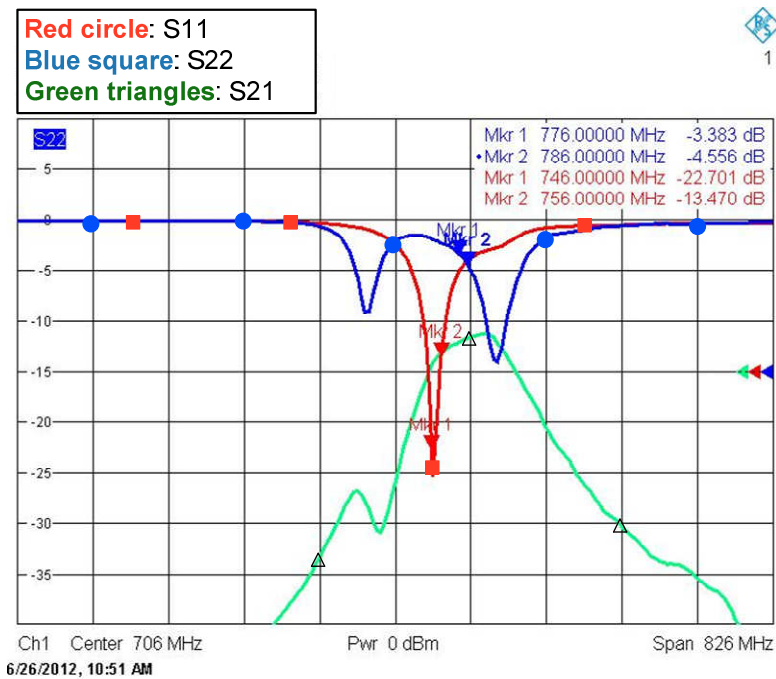
Characteristic	Simulated Values (dB)	Measured Values (dB)
Reflection Coefficient in Uplink band	$-11.3 < S_{11} < -6.4$ $-9.4 < S_{22} < -5.6$	$-5.5 < S_{11} < -4.6$ $-4.5 < S_{22} < -3.3$
Reflection Coefficient in Downlink band	$-11.7 < S_{11} < -7.5$ $-9.2 < S_{22} < -6.1$	$-22.7 < S_{11} < -13.4$ $-2.2 < S_{22} < -3$
Mutual Coupling in Uplink Band	$-8.2 < S_{21} < -6.9$	$-13 < S_{21} < -11.5$
Mutual Coupling in Downlink Band	$-8.7 < S_{21} < -7.3$	$-15 < S_{21} < -13.4$
Maximum Gain Antenna #1	-0.07	0.19
Maximum Gain Antenna #2	-2.1	-11
Antenna #1 Radiation Efficiency	62.8%	48%
Antenna #2 Radiation Efficiency	46%	38%

Table 2.5 Dependence of LTE-Band 13 PIFAs on Phase Difference between Antennas.

Characteristic	Simulated Values (dB)		
	0	$\pi/2$	π
Phase Difference	0	$\pi/2$	π
Max. Gain	-7 dB	-1.11 dB	0.28 dB
Radiation Efficiency	23.1%	59%	76.6%



(a)



(b)

Fig. 2.10 The S-Parameter for the Antennas of the LTE-B13 Handset (a) Simulation results (b) Measurement results.

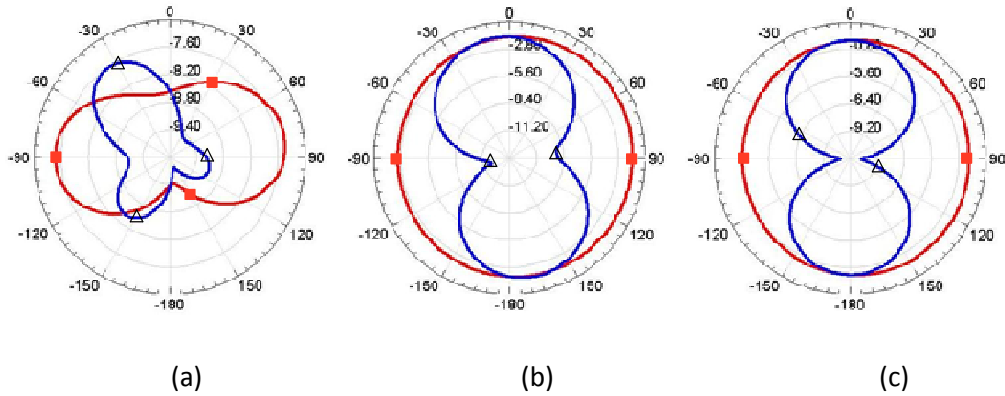


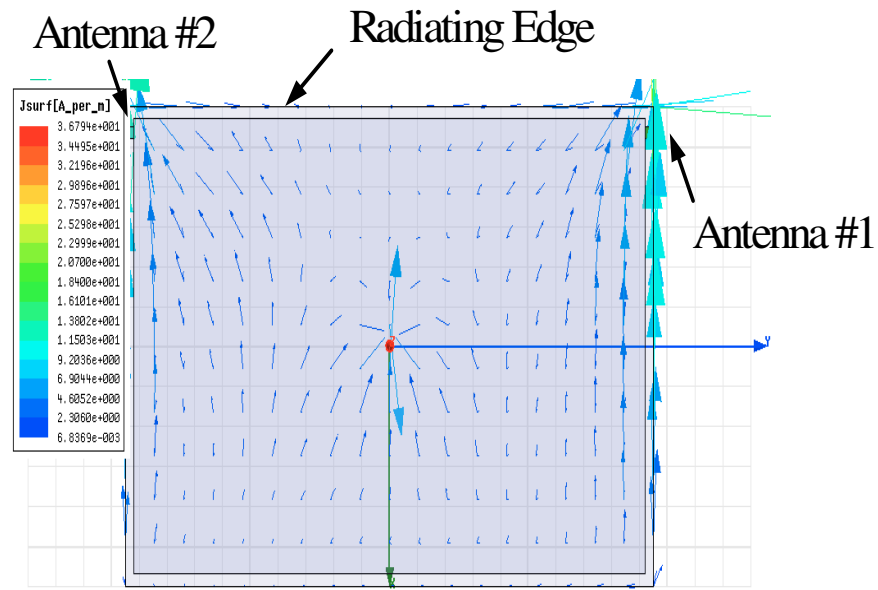
Fig. 2.11 The Simulated Radiation Patterns of the LTE-Band 13 PIFAs in $\phi=0$ (red square) and $\phi=90$ (blue triangle)-planes in Scenario 1 when the feeding phase difference is: (a) 0 (b) $\pi/2$ (c) π .

Table 2.6 Simulated and Measured Performance of LTE-Band 13 Handset Antennas in Scenario 2.

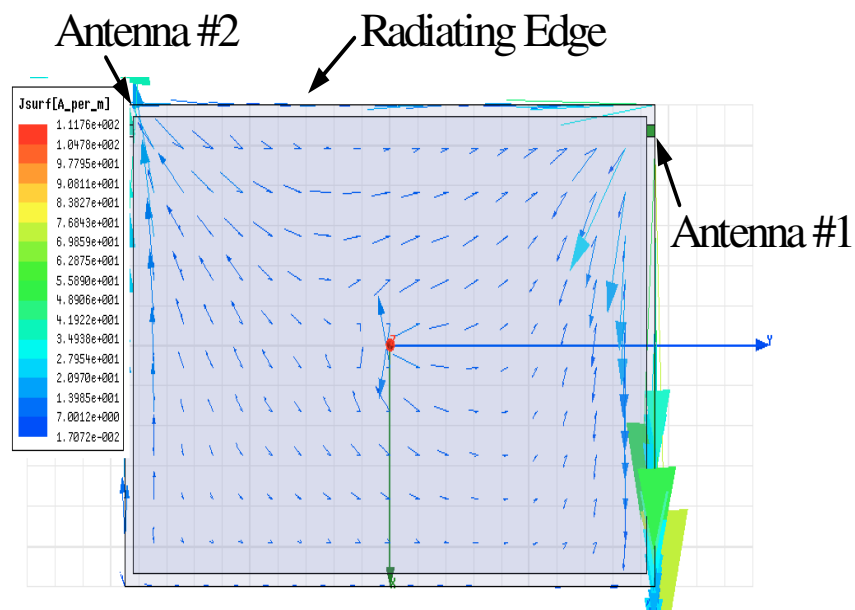
Characteristic	Simulated Values (dB)	Measured Values (dB)
Max. Gain	-0.82 dB	0.19 dB
Radiation Efficiency	62.1%	48%

Table 2.7 Simulated and Measured Performance of LTE-Band 13 Handset Antennas in Scenario 3.

Characteristic	Simulated Values (dB)	Measured Values (dB)
Max. Gain	-2.1 dB	-11 dB
Radiation Efficiency	46.5%	38%

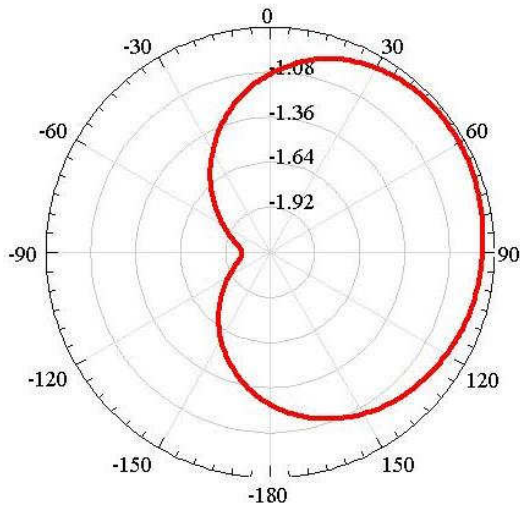


(a)

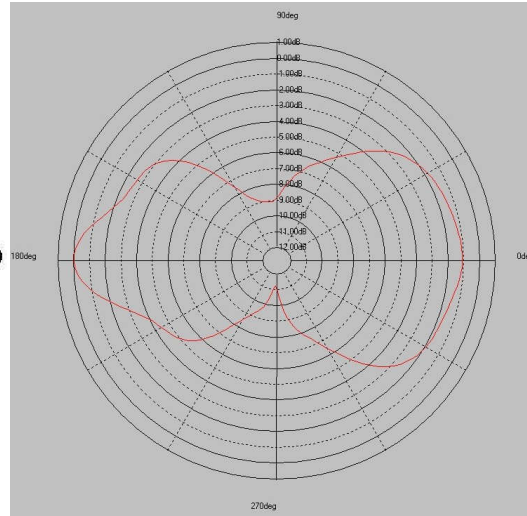


(b)

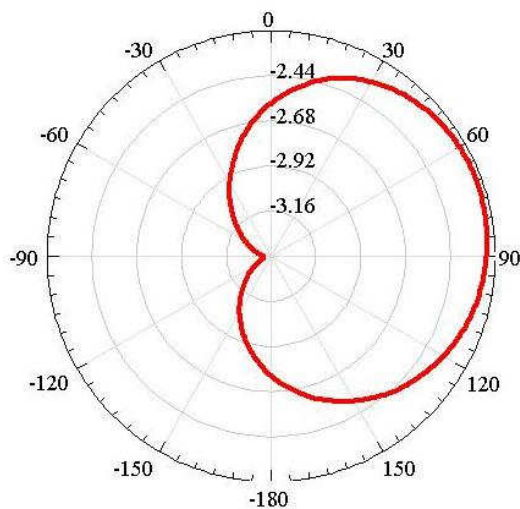
Fig. 2.12 The Ground Current Distribution on the LTE-Band 13 Handset (a) When the phase difference is set to zero. (b) When the phase difference is set to 180 degrees.



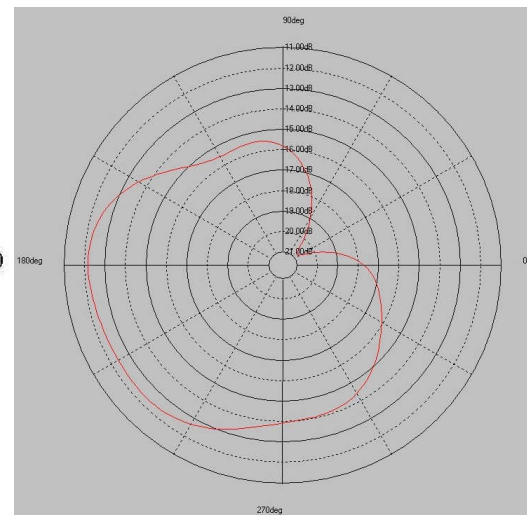
(a)



(b)



(c)



(d)

Fig. 2.13 The Radiation Pattern of the semi-populated GSM-900 handset antennas at 925 MHz ($\phi=0$ plane) (a) Simulation result for Antenna #1 (Scenario 2) (b) Measured result for Antenna #1 (Scenario 2) (c) Simulation result for Antenna #2 (Scenario 3) (d) Measured result for Antenna #2 (Scenario 3).

2.4 Conclusion

This chapter presents a design methodology for the Printed Inverted-F Antenna. The antennas radiate through the interaction of the antenna structure with the ground plane. The radiation characteristics can be controlled by four geometrical parameters of the antenna layout while being dependent on the size of the ground plane as well.

The methodology presented is applied to the design of multiple antennas on a semi-populated handset model at three different telecommunication frequencies, i.e., the GSM-1800, GSM-900 and LTE-Band 13. A two-step design process is used to investigate the effects of other components, namely the LCD screen and battery, on the antennas. The final designs achieve the resonance frequency, bandwidth and reflection coefficients required for operation in the respective bands. Simulations reveal the degradation in the radiation performance caused by the presence of the two considered components.

The results for the GSM-1800 antennas reflect the high gain and efficiency that a PIFA is capable of reaching if it is positioned on a sufficiently large ground plane. The results for the GSM-900 and LTE-Band 13 antennas highlight this point further. These two handset antennas are unable to achieve the same performance levels as the GSM-1800 design due to the smaller electrical size of the ground plane at those frequencies. Simulations demonstrate that the

radiation pattern, gain and efficiency of the LTE-B13 handset is dependent on the phase difference between the feeds of the antennas.

The fabricated models GSM-1800 and GSM-900 handset prototypes met the operational targets for their respective bands. One of the fabricated LTE-B13 handset antennas showed discrepancy from the simulated results whereas the other antenna performed as expected. This can be attributed to fabrication and measurement errors. All three designs nevertheless satisfy the operational targets set for the respective bands except for the mutual coupling requirements. Chapter 3 investigates the paths through which the mutual coupling occurs and Chapter 4 discusses different methods that can be used to reduce coupling.

Chapter 3

Mutual Coupling Between Two Antennas on a Semi-Populated Handset

3.1 The Definition of Mutual Coupling

When two or more antennas are placed in close proximity to one another, electromagnetic (EM) fields emitted by one antenna is received by the other antennas even if they are not the intended recipients [47]. This interaction between the antennas is referred to as mutual coupling. The author of [52] refers to the transmitting antenna as the “aggressor antenna” and the non-intentional recipient as the “victim antenna”. Using this nomenclature, the non-intentional reception of the EM fields causes a current distribution to be set up on the victim antenna that interferes with the victim’s own current distribution due to its excitation. This interaction changes the radiation performance of the victim antenna and must be taken into account when designing a multi-antenna system.

It should be noted that the degradation of the radiation pattern due to mutual coupling has repercussions for other systems on the handset as well. The battery life for example decreases because of the larger amount of power required to



Fig. 3.2: The Definition of Scattering Parameters for a two Antenna System.

compensate for a reduced gain antenna system. It is therefore vital to identify, understand and, if possible, reduce the mutual coupling.

Antenna engineers commonly use the scattering matrix to define mutual coupling. The scattering matrix of a two-antenna system is defined as [53]:

$$\begin{bmatrix} b_1 \\ b_2 \end{bmatrix} = \begin{bmatrix} S_{11} & S_{12} \\ S_{21} & S_{22} \end{bmatrix} \begin{bmatrix} a_1 \\ a_2 \end{bmatrix} \quad \text{Eq. 3.1}$$

Where the parameters $b_{1,2}$ and $a_{1,2}$ represent power waves, as shown in Figure 3.1. The term S_{21} in this matrix represents the ratio of the power captured by Antenna #2 to the power transmitted by Antenna #1 when Antenna #2 is terminated to a matched load. This is consistent with the definition of mutual coupling presented in [54]. Hence, the mutual coupling between two or more antennas can be found using Vector Network Analyzer (VNA) measurements as it was done in the investigation presented in Chapter 2.

3.2 The Factors Responsible for Mutual Coupling

The definition of mutual coupling presented in the previous section is deceptively simple because there are several contributing factors that determine the value of the coupling.

The coupling between two antennas also depends on the reflection coefficients of the two antennas and this is implicit in Equation 3.1; if the two antennas are designed to operate at different resonance frequencies, the coupling between them might be negligible, even if they are placed close to one another. If the antennas do not have a good matching profile, the coupling may seem to be misleadingly low due to the large reflected power at the excitation ports that leaves little power for transmission in between. This is why in all the designs presented in Chapter 2, meeting the target S_{11} limit was made the first priority.

The coupling also depends on the distance between the antennas. If they are placed too close together, they may begin to experience high coupling through near-field interactions. The authors of [37] suggest that this can be determined by increasing the distance between them. If the coupling is caused by near-field coupling, its value will fall by 12 or 18 dB when the distance between the antennas is doubled. If it is caused by far-field coupling, the coupling will reduce by 6 dB when the distance is doubled. The antennas in this

thesis were all determined to couple through far-field interactions by doubling the distance between the antennas and observing a 6 dB decrease in mutual coupling.

Other than far-field radiation, two antennas may interact if they share a common substrate and/or a ground plane through the substrate-bound modes including slow waves and parallel plate modes. For example, the substrate may support slow wave modes, that propagate at a slower rate than space-waves, and couple antennas or in general any components found on the same substrate [55]. Systems may be designed that either intentionally excite such modes, such as in antenna miniaturization [56] or aperture-coupled feed systems [57], or stop such modes from propagating [55, 36].

Common ground plane can be considered in the context of common substrate model investigations. Certain research works put more emphasis on observation of current distribution on the common ground plane. For example, the authors of [58] show that if antennas are placed too close together on a small ground plane, the mutual coupling increases significantly even if the antennas do not operate in the same frequency bands.

Another factor that contributes to mutual coupling is the fact that other components, such as those considered in this thesis, are capable of receiving and re-transmitting EM waves. This “scattered” radiation [31] may not be as

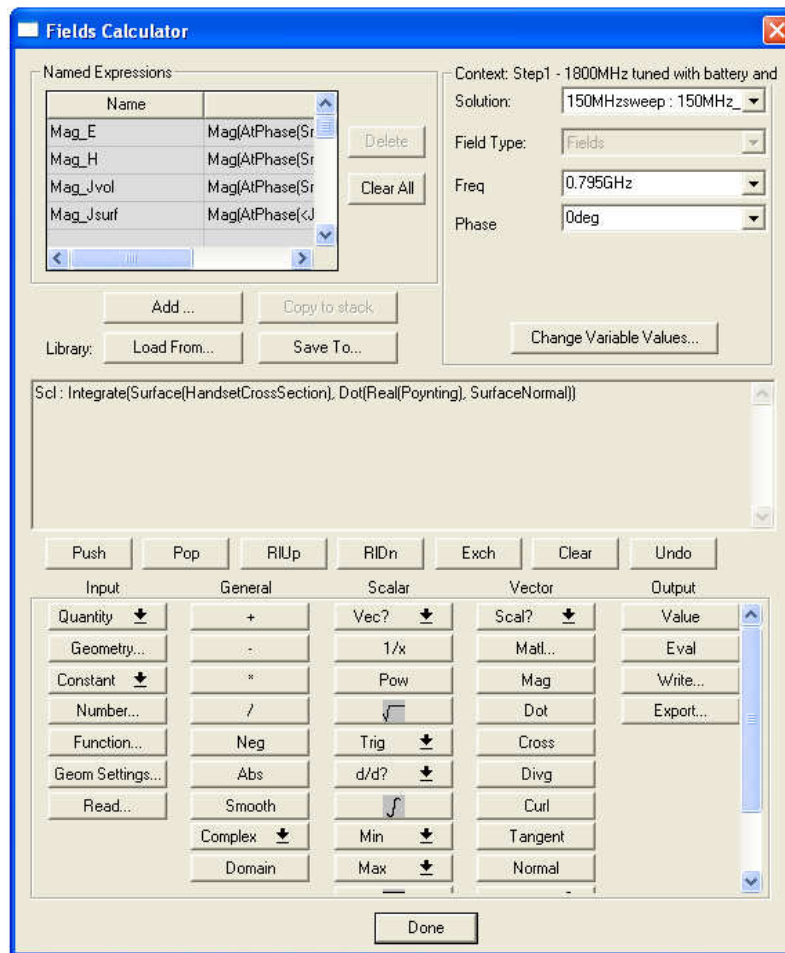


Fig. 3.3 The Field Calculator in the Ansoft HFSS Ver. 12 software.

strong as the aggressor antenna's radiation but must nevertheless be considered.

3.3 Simulation Setup

The various mutual coupling mechanisms outlined in the previous section are extremely difficult (and sometimes impossible) to formulate analytically. This is

because of the large and complex relationships that exist for the interactions between the substrate, ground, components and antennas. Physically measuring these interactions is also a daunting task since any ports or test-fixture incorporated in the handset to measure the coupling introduces a coupling factor of its own that will alter the coupling factors for the other components. To solve this seemingly impossible task, numerical methods can be employed to gain an insight into the mechanisms responsible for antenna coupling.

The simulations presented in this chapter are carried out by using the Ansoft HFSS Version 12 software. Using this software, it is possible to calculate the power flowing through a user-defined cross-sectional area of a model. The power, P , flowing through an area A can be defined as:-

$$P = \int S \cdot A \, dA \quad \text{Eq 3.2}$$

where S is the Poynting vector and is defined by [59]:

$$S = \frac{1}{2} \text{Re}(E \times H^*) \quad \text{Eq. 3.3}$$

Where E is the Electric Field and H is the Magnetic field. The HFSS simulation software provides a field calculator which allows one to calculate Equation 3.2 for any user-defined area. A snapshot of the field calculator is shown in Figure 3.2. The field calculator is employed to determine whether the mutual coupling between the handset antennas is dominantly caused by space-

radiation or by handset-bound modes. Two cross-sectional areas are therefore defined for the semi-populated handset models. The first, labeled “Handset cross section” and shown in Figure 3.3, is positioned to be equally spaced from the two antennas. As the name suggests, this cross-section captures the power flow through the handset’s cross-sectional area. The second surface, labeled “Space Cross-Section” and shown in Figure 3.4(a) and Figure 3.5(a), is a cross-section that extends from the handset to the top and bottom boundary walls of the simulated volume (in HFSS these boundaries are defined as radiating boundaries). The Space Cross-Section takes the same position (i.e., overlaying xz or yz planes) as the Handset Cross-Section. It should be noted that the Space cross-section does not overlap with the Handset Cross-section, as highlighted in Figure 3.4 (b) and Figure 3.5 (b).

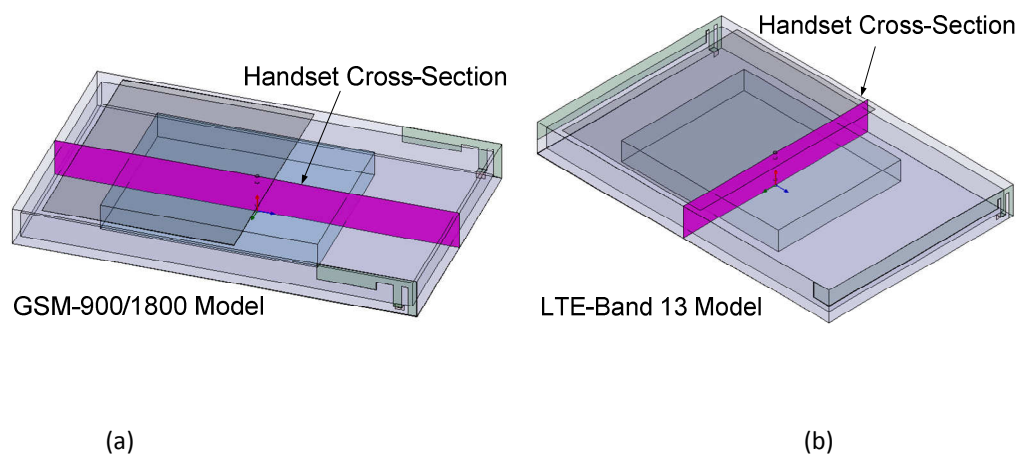


Fig. 3.4 The “Handset Cross Section” Area defined for (a) the GSM-900/1800 Models (b) LTE-Band 13 Model.

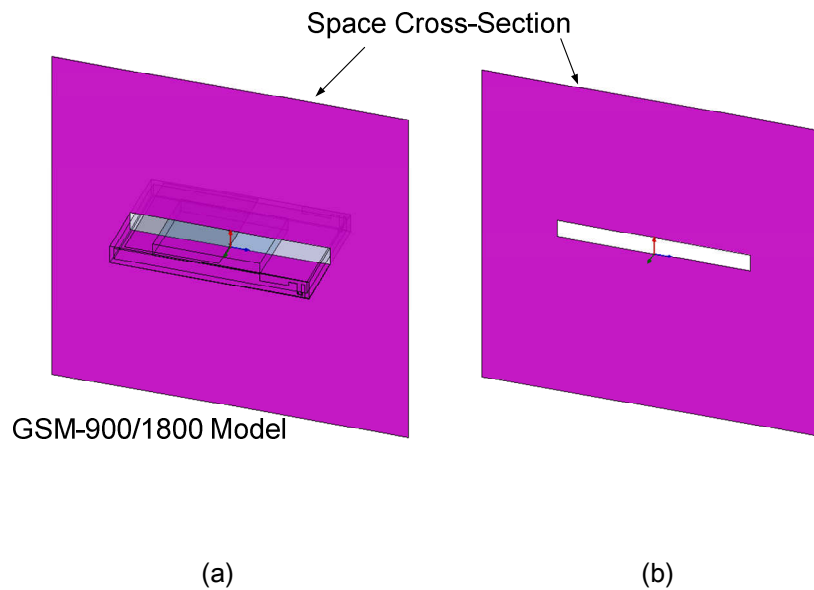


Fig. 3.6 The “Space Cross Section” Area defined for the GSM-900/1800 Models (a) The orientation of the Space cross section with respect to the handset (b) The Space cross section with the handset hidden from view.

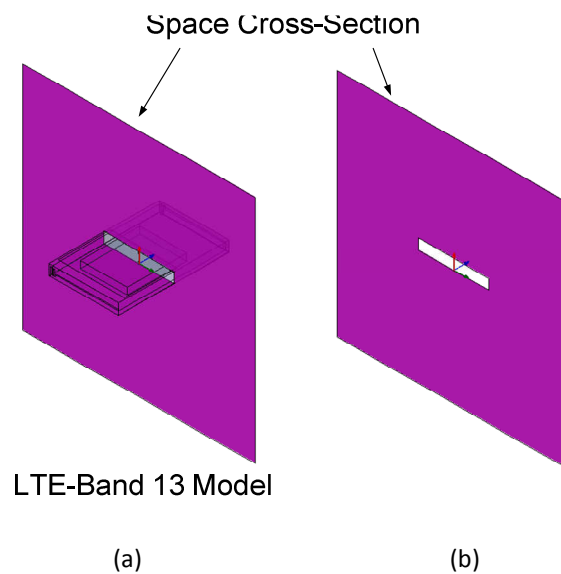


Fig. 3.5 The “Space Cross Section” Area defined for the GSM-900/1800 Models (a) The orientation of the Space Cross Section with respect to the handset (b) The Space Cross Section with the handset hidden from view.

3.4 Results

Each antenna was fed using a 50Ω lumped port with a power of 1 Watt, and the amount of power that was coupled between the antennas was calculated using the field calculator. To have a fair comparison, the calculated power was normalized and the results are presented in Table 3.1 and plotted in Figure 3.6.

It can be seen that for the GSM-1800 and GSM-900 models, the amount of power that flows through the Handset Cross-Section is less than the amount that flows through the Space Cross-Section. This indicates that the mutual coupling between the antennas takes place predominantly through a non-substrate bound (space-wave) mechanism.

Table 3.2 Mutual Coupling Profile Simulation Results.

Model	Handset Cross Section	Space Cross Section
GSM-1800 Model	19.3%	80.7%
GSM-900	16.7%	83.2%
LTE-Band 13	88.1%	11.9%

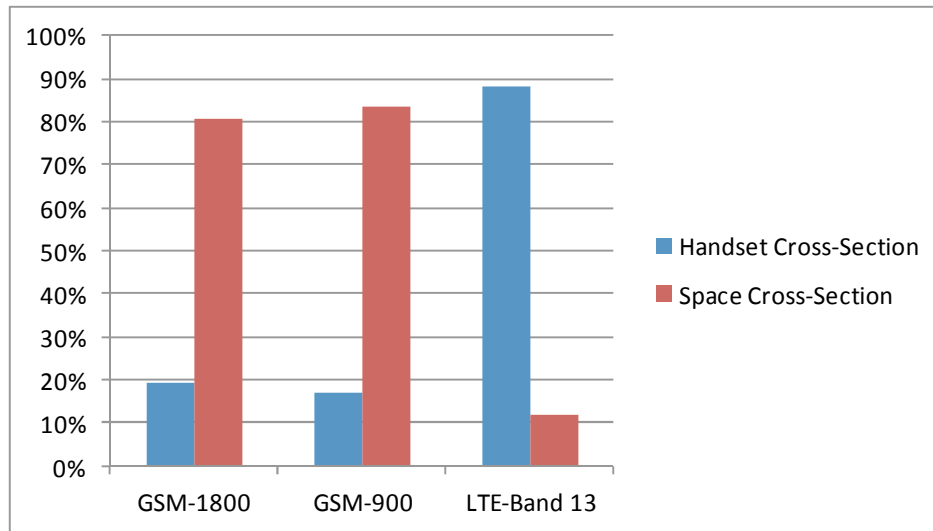


Fig. 3.7 The Results of the Mutual Coupling Profiles for the three Handsets.

The LTE-Band 13 model however exhibits a different mutual coupling profile. The amount of power that is going through the Handset Cross-Section is significantly higher than the amount of power that goes through the air. This is opposite to the results for the GSM-900/1800 model. The results from Chapter 2 demonstrated the relationship between the radiation characteristics of the handset and the current distribution on the ground plane of the LTE-B13 handset. The increased mutual coupling through the handset may be attributed to the stronger contribution of the current distribution on the ground plane to the overall radiation. To investigate the accuracy of this observation, methods that reduce the current distribution on the ground plane are investigated in the next chapter.

Chapter 4 also explores other methods to tackle each type of coupling mechanism for the other handsets and investigates whether or not they can be readily applied to the handset model.

3.4 Conclusion

This chapter presented a numerical technique to evaluate the mutual coupling between two PIFAs placed on a semi-populated mobile handset model. Using a commercially available Electromagnetic solver, the mutual coupling was found to be caused predominantly through space-bound fields for the GSM-900 and GSM-1800 handset antennas. The coupling between the LTE-Band 13 handset antennas on the other hand was determined to be more significantly due to handset-bound modes.

Chapter 4

Mutual Coupling Reduction Techniques

4.1 Introduction

The previous chapters investigated the radiation characteristics of two PIFAs on a semi-populated handset at three different operating frequencies. The mutual coupling was found to exceed the performance target set at each of the three frequency bands. Having determined in Chapter 3 whether the coupling between the antennas was dominated by handset-bound or space wave modes, an investigation is carried out in this chapter on methods to reduce the coupling.

This chapter begins by presenting a survey of mutual coupling reduction methods in Section 4.2. Section 4.3 discusses the suitability of these methods to the mobile handset being investigated and the results of the ultimately chosen technique are presented in Section 4.4. This is followed by conclusions in Section 4.5.

4.2 Overview of Mutual Coupling Reduction Techniques

Obviously if two antennas are placed as far from each other as possible the interaction between them is weakened, but this is not feasible in compact and integrated systems. The first technique that can be used for coupling reduction is by using the inherent nulls in the radiation patterns of the receiving and transmitting antennas [60]. Therefore, it is possible to orient and position the victim (or aggressor) antenna on the handset so that it faces the radiation null of the aggressor (or victim) antenna. The authors of [34] carried out such an investigation for two PIFAs operating on a common ground plane. They concluded that the mutual coupling between the antennas is minimized when the two antennas are placed at the opposite ends of the shared ground plane due to having polarization mismatch.

A second method to enhance isolation in multi-antenna systems uses a parasitic radiator (or coupler) to counteract the effect of the aggressor antenna on the victim antenna as presented in [35]. The parasitic radiator, that is placed between the two antennas, is designed to receive the EM fields from the aggressor antenna and then re-emit compensating fields. Hence, the victim antenna is affected by two sources, i.e., the aggressor and the parasitic element. The parasitic element should be designed and positioned so that the currents induced by the two sources cancel each other on the victim antenna to the extent

possible. Because of the fact that the parasitic element re-emits the induced field by the aggressor antenna, the two currents on the victim antenna do not have equal amplitudes and are out of phase resulting in a decreased coupling factor. A theoretical approach to extend this method to any antenna configuration is provided in [61].

The authors of [37] investigated the source of coupling in patch antennas. They identified the polarization currents beneath the patch as the source of unwanted EM radiation and suggested using shorting pins to cancel polarization currents. Their method reduces the patch coupling by 15 dB. The authors of [62] present another method to reduce the coupling between two patch antennas. Their technique involves the physical modification of the substrate beneath the patch antennas by etching selective grooves to remove the polarization currents.

In reference [63] a mutual coupling reduction method is presented by introducing a negative group delay in the feeds of two meandered monopole antennas. Another method that focuses on the feed network is presented in [64], which uses a modified feed network to induce an even mode on one meandered monopole antenna and an odd mode on another. This results in a 10 dB reduction in mutual coupling while the radiation efficiency remains unchanged.

Another technique is presented by the authors of [65] where a metallic line is used to join two parallel meandered monopole antennas. The metallic line is

positioned so that it generates a reactive impedance to cancel the capacitance created by the two closely-placed and parallel antennas. This technique results in an increase of 10 dB in antenna isolation.

The authors of [38] modify the common ground plane to reduce the mutual coupling between closely spaced antennas. Two slots are introduced between two patch antennas on the common ground plane. The length of each slot is equal to half the operating wavelength in free space. The slots reduce the coupling by introducing a phase difference between the surface currents induced by each antenna on the ground plane. This causes the currents to cancel partially or completely (depending on their positioning) and allows for the antennas to decouple from one another on the ground plane by up to 35 dB .

Another form of ground modification is presented in [39] which employs a dumb-bell shaped slot between two patch antennas. The slot creates a bandstop filter that prevents current propagation in a particular frequency band. By changing the layout dimensions, the filter can be optimized to reduce the antenna coupling at a desired band.

The concept of using a structure to act as a bandstop filter is not unique to ground slots only. The authors of [40] present a three dimensional structure called an Electromagnetic Band-Gap structure (EBG) for this purpose. An EBG configuration consists of a basic structure, called the unit cell, which is

periodically repeated. Numerous designs for EBG structures have been introduced in the past three decades as they have been gradually introduced in different applications. In this thesis, the mushroom-type designs that were presented by Sievenpiper et al. in [40] and extended for electromagnetic interference (EMI) reduction by Abhari et al. in [66], are employed for antenna isolation. The unit cell of a mushroom-type EBG structure consists of a metallic patch that is connected to a common ground plane through a metallic via. It should be mentioned that it is possible to create an EBG structure without using vias as well (but it will not be called a mushroom-type EBG structure). The authors of [67] present a summary of four different designs for EBG structures that do not use vias.

In reference [68] utilized a mushroom EBG structure is utilized to improve isolation in a multi-antenna system. The EBG arrays are positioned between and around two parallel slot antennas operating at 5.2 GHz to improve antenna isolation by 28 dB.

4.3 Mutual Coupling Reduction Techniques for a Mobile Handset

When discussing the suitability of a certain mutual coupling reduction technique for a mobile handset several factors must be taken into consideration.

The technique must effectively increase antenna isolation while maintaining acceptable radiation characteristics. Therefore, a method that may improve the antenna isolation should only be considered when the benefits outweigh the possible performance degradations.

The technique put forward in [34] for example is rather simple and elegant, since it requires no modification to the structure other than the placement and orientation of the antennas. This technique however is not suitable to apply to the handset being investigated in this thesis. The results from Chapter 2 concluded that the LCD screen and battery impact the radiation performance of the antennas. To counter this, the PIFAs in the GSM-900 and GSM-1800 designs are positioned as far away from these components as possible. It is not possible to position the GSM-900 and GSM-1800 PIFAs orthogonally on opposite walls of the handset without placing one of the antennas closer to the components. For this reason, for the LTE-Band 13 design, Antenna #1 was placed at the bottom of the handset. Changing its orientation reduces antenna isolation and the radiation performance of the system suffers as a result. This technique is therefore not a viable option for the handset at any of the frequency bands.

The method suggested in [35, 69] on the other hand can be implemented on the handsets and is discussed further in Section 4.4.1. This technique unfortunately cannot be extended to the LTE-Band 13 handset because of the

relatively large size of the parasitic radiator. At the LTE-Band 13, the parasitic radiator occupies a similar foot-print as that of the PIFAs causing it to overlap with the LCD screen. Section 4.4.1 therefore presents the implementation of the parasitic radiator coupling reduction technique at the GSM-900 and GSM-1800 frequencies only.

It should be mentioned that instead of inserting a parasitic printed monopole between the PIFAs it is possible to create a similar effect by etching a slot antenna on the ground plane [38]. However, this technique is not generally preferred due to increasing back radiation (directed towards user) and potential compromising of signal and power integrity. For the sake of thoroughness, this technique is applied to the GSM-1800 mobile handset to test its feasibility and is presented in Section 4.4.2.

The Electromagnetic Band-Gap structure of [40] does not suffer from this problem since it contains a solid ground plane underneath. The unit cell of the EBG structure can be made small enough to fit within the limited volume available. The EBG structure can be designed as an omnidirectional filter with strong attenuation properties to reduce mutual coupling. This 2D filter dominantly impacts mode propagation in the substrate and is therefore ineffective in reducing coupling via space-wave modes. Since the GSM-1800 model falls into

this category, the EBG investigated in Section 4.4.3 is analyzed for the GSM-900 and LTE-Band 13 handsets only.

Other methods for isolation improvement such as [36] in which grooves are etched underneath the patch antennas or [37] where shorting pins are strategically placed to eliminate polarization currents underneath the patch antenna are not investigated in this thesis because they target patch antennas specifically. Their application to cellular mobile handset PIFAs is not within the scope and time frame of this thesis.

4.4 Investigation of Antenna Coupling Reduction Techniques in a Semi-Populated Handset

4.4.1 Investigation of a Bent Monopole Parasitic Radiator for a Mobile Handset

To investigate the method presented in [35], a parasitic radiator is placed on the bottom side of the handset, as shown in Figure 4.1. The radiator takes the form of a bent monopole. In order to position the monopole as far from the LCD screen and battery as possible, it is desirable to shorten the physical length of the monopole. The method suggested by the author of [44] is employed here for this purpose; a capacitive load is added to the monopole to shorten its length. Starting with the GSM-900 handset parasitic monopole first, a lumped capacitor

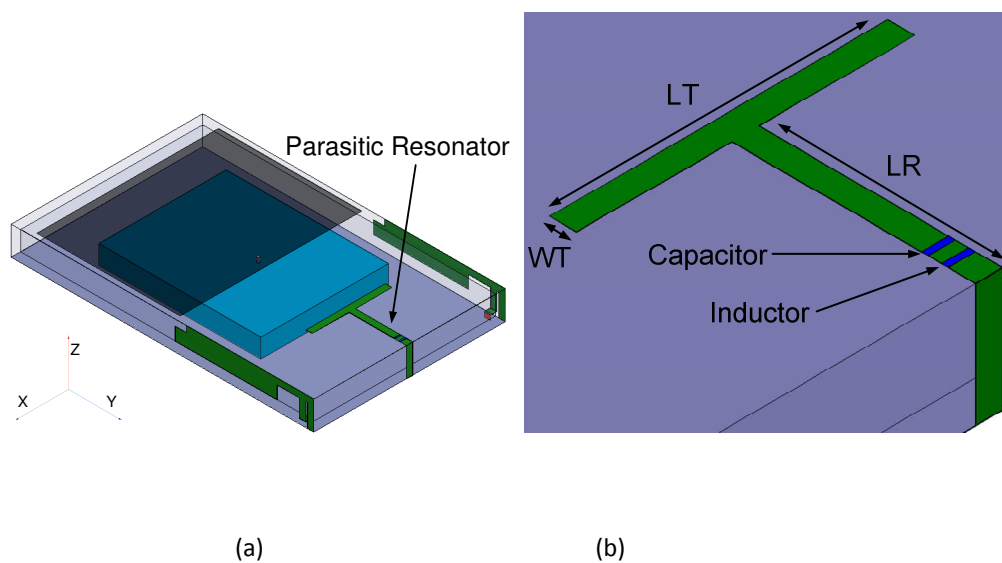


Fig 4.1 (a) 3D view of the placement of the parasitic radiator between the two antennas (b) The layout parameters of the parasitic radiator.

Table 4.1 Dimensions of Parasitic Radiator.

Parameter	GSM-1800	GSM-900
LR	7.5 mm	25 mm
LT	5 mm	25 mm
WT	2 mm	3 mm
Capacitance	4.5 pF	4 pF
Inductance	10.5 nH	10 nH

is added to the monopole. The capacitor is given an initial value of 1 pF and the capacitance is increased until the length, LR, of the monopole is small enough to be sufficiently isolated from the battery and LCD screen. The size of the monopole is further reduced by adding a top section resulting in T-shaped bent monopole. The resonance frequency of the monopole is inversely proportional to the length, LT, of the top section. The length LT is increased until the desired resonance frequency for the bent monopole is obtained.

The introduction of the capacitive load shortens the physical length, LR, and changes the input impedance of the monopole as well. In order to cancel the reactive impedance introduced in this manner, a lumped inductor is inserted in the monopole. Once the values for the capacitor and inductor are finalized through full-wave optimizations for the GSM-900 handset, the process is repeated for the GSM-1800 MHz handset.

The final values obtained for each band are presented in Table 4.1. It should be noted that the authors of [69] report a similar investigation, with the lumped impedances replaced by varactors which allows for the parasitic radiator to become tunable.

In this thesis, the first investigation of this topic was carried out at the GSM-1800 band. The simulated results reveal that the radiator is not effective in reducing the coupling below the required level (-15 dB) of either the uplink or the downlink band. The reflection coefficients and mutual coupling for the GSM-1800 handset with parasitic radiator is shown in Figure 4.2(a). The resonance frequency of both antennas shifts from 1.8 GHz to 1.75 GHz. The bandwidth for the PIFAs also decreases from 186 MHz to 170 MHz. Due to the shift in resonance frequency and the decrease in bandwidth, the PIFAs are no longer able to cover both uplink and downlink bands.

Figure 4.3 shows the radiation pattern at the $\Phi=0$ cut-plane for the GSM-1800 PIFAs with and without the parasitic radiator. The radiation patterns for the PIFAs do not show a dramatic change when the parasitic radiator is added because the radiator has a narrow bandwidth of approximately 50 MHz.

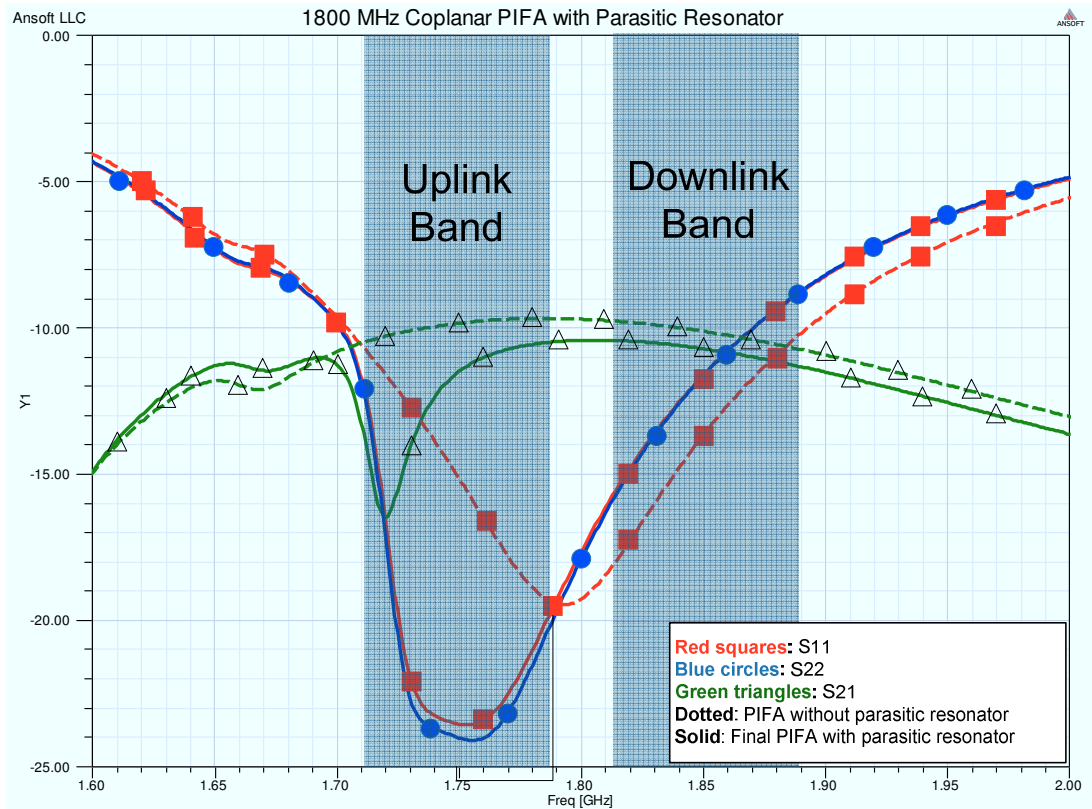
Methods to extend the bandwidth of the mutual coupling reduction technique must be applied in order to cover both bands. One of these techniques is based on employing multiple parasitic resonating elements. This however would pose a

new problem, since the only available space is the limited board area between the two antennas. Implementing the multi-element parasitic design requires further investigations on component placement and coupling reduction and layout optimizations which are not within the scope of this thesis. Therefore the single parasitic radiator is concluded not to be a feasible solution for the GSM-1800 handset model.

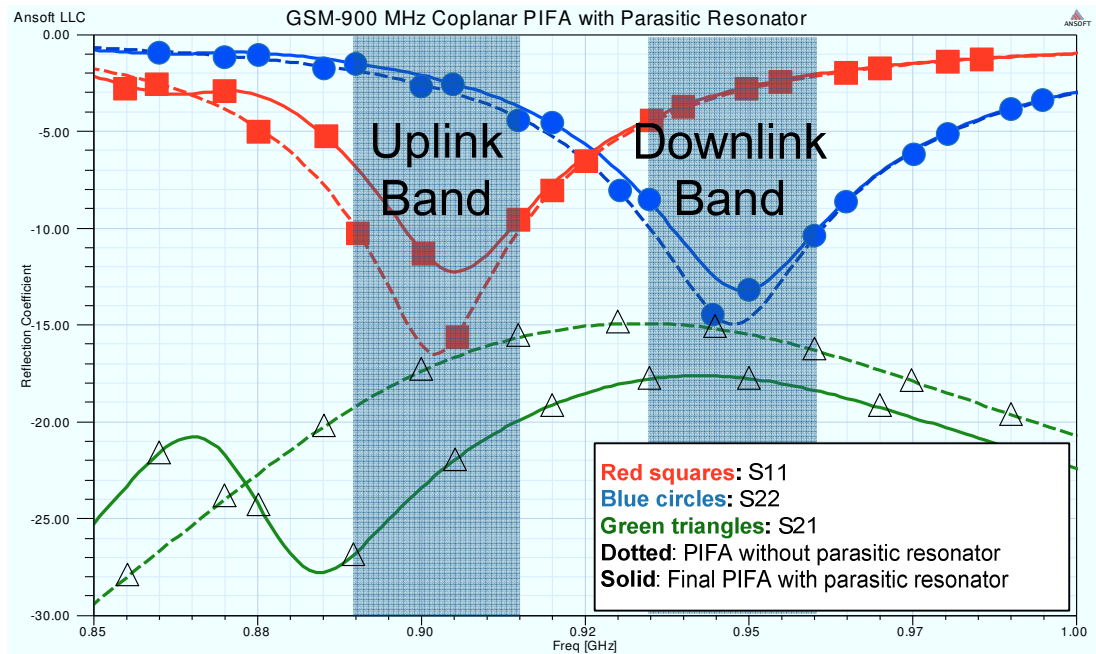
The second investigation was carried out at the GSM-900 band. The simulated S-parameters are shown in Fig. 4.2(b). The reflection coefficients are summarized in Table 4.2 and show that they decrease slightly but there is no shift in the resonance frequency. The radiator is also able to reduce the mutual coupling below the -15 dB level required across both bands.

The radiation patterns, depicted in Figure 4.4 show the radiator causes the maximum gain of the antenna system at 900 MHz to drop. The gain for Antenna #1 falls from 0.36 dB to -1.1 dB and from -0.02 dB to -2.1 dB for Antenna #2. The radiation efficiencies are also reduced when the parasitic radiator is added. The radiation efficiency of Antenna #1 falls from 67.7% to 53% and from 69.9% to 53.4% for Antenna #2.

This however is expected since the parasitic radiator antenna, as the name suggests, obtains its radiating power from the two main antennas thereby reducing the power that would otherwise be transmitted to other systems.



(a)



(b)

Fig 4.2 The S-Parameters for (a) GSM-1800 handset with and without parasitic radiator (b) GSM-900 handset with and without parasitic radiator.

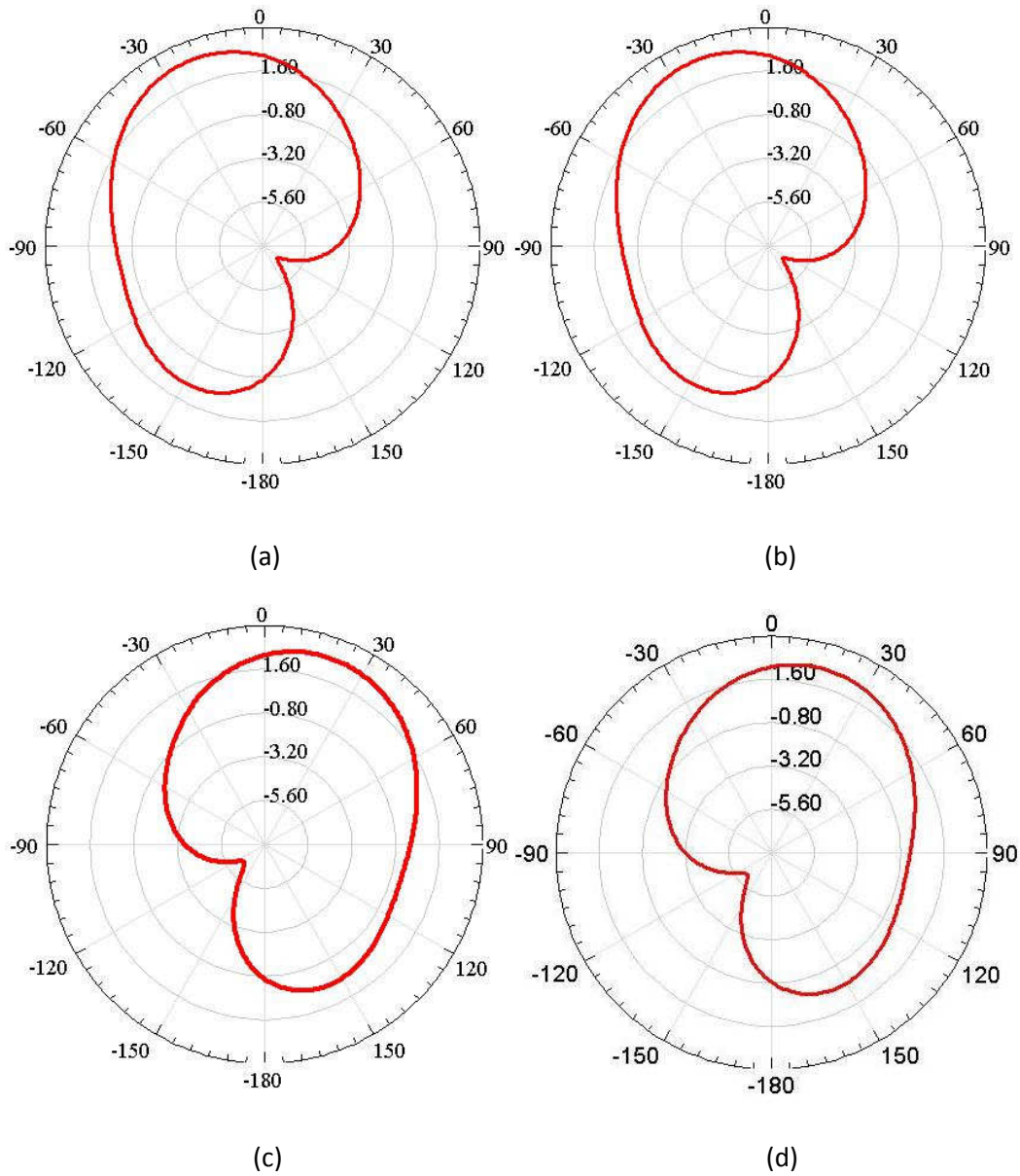


Fig 4.3 The Radiation Pattern of the semi-populated GSM-1800 handset antennas at 1.8 GHz ($\varphi=0$) (a) Simulation result for Antenna #1 without parasitic radiator (b) Simulation result for Antenna #1 with parasitic radiator (c) Simulation result for Antenna #2 without parasitic radiator (d) Simulation result for Antenna #2 with parasitic radiator.

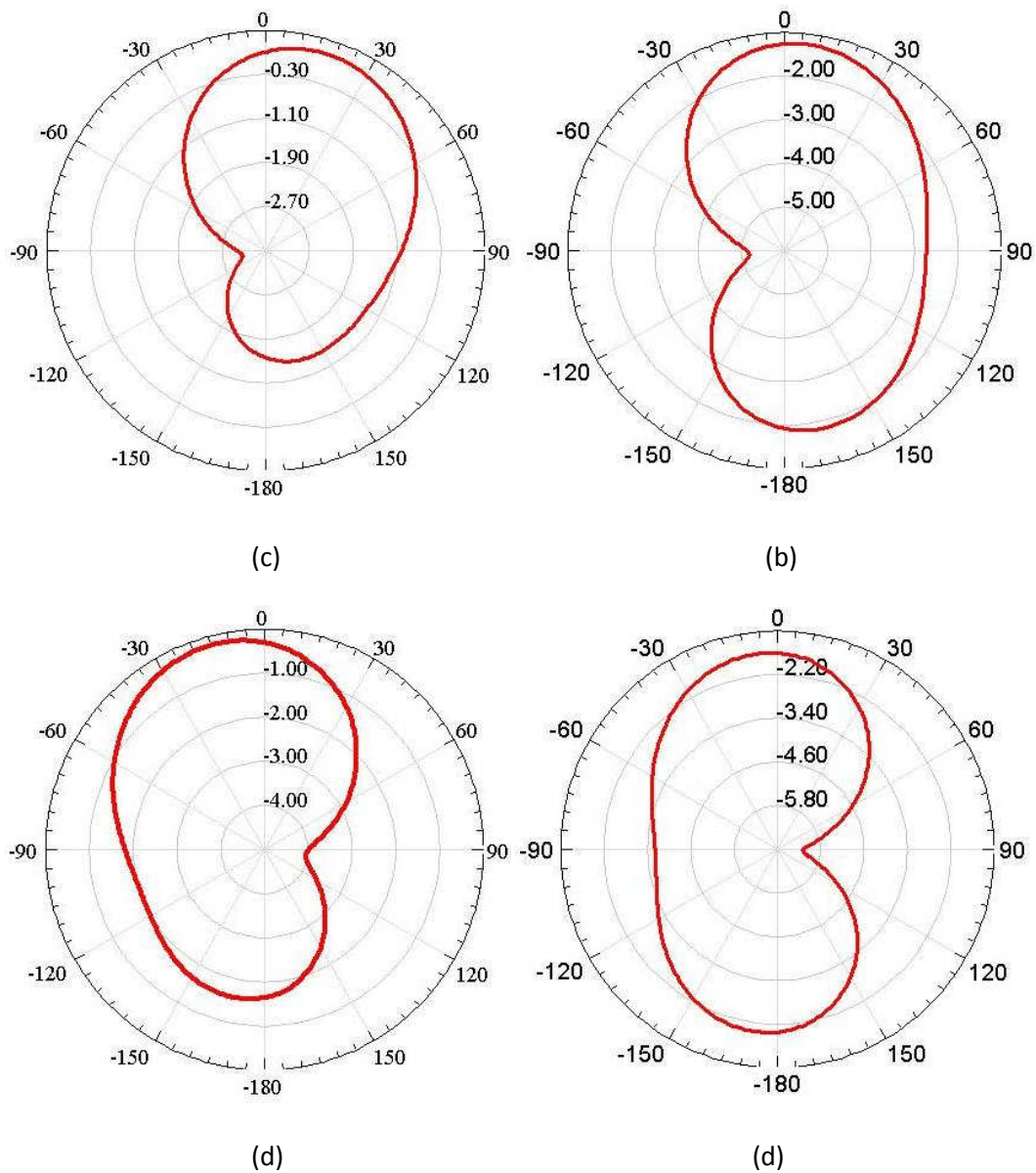


Fig 4.4 The Radiation Pattern of the semi-populated GSM-900 handset antennas at 925MHz ($\varphi=0$) (a) Simulation result for Antenna #1 without parasitic radiator (b) Simulation result for Antenna #1 with parasitic radiator (c) Simulation result for Antenna #2 without parasitic radiator (d) Simulation result for Antenna #2 with parasitic radiator.

Table 4.2 Simulated Performance of Antennas for GSM-900 Handset with and without parasitic radiator

Characteristic	Without Parasitic Radiator (dB)	With Parasitic Radiator (dB)
Reflection Coefficient in Uplink band	$-16 < S_{11} < -10$	$-12 < S_{11} < -7$
Reflection Coefficient in Downlink band	$-15 < S_{22} < -10$	$-14.3 < S_{22} < -8.5$
Mutual Coupling in Uplink Band	$-19.1 < S_{21} < -15.5$	$-27 < S_{21} < -20$
Mutual Coupling in Downlink Band	$-16 < S_{21} < -14.7$	$-16.8 < S_{21} < -16.2$

4.4.2 Investigation of a Ground Slot Parasitic Radiator for a Mobile Handset

The parasitic radiator for this method is formed by introducing a slot on the ground plane between the two antennas, as shown in Figure 4.5. The length of

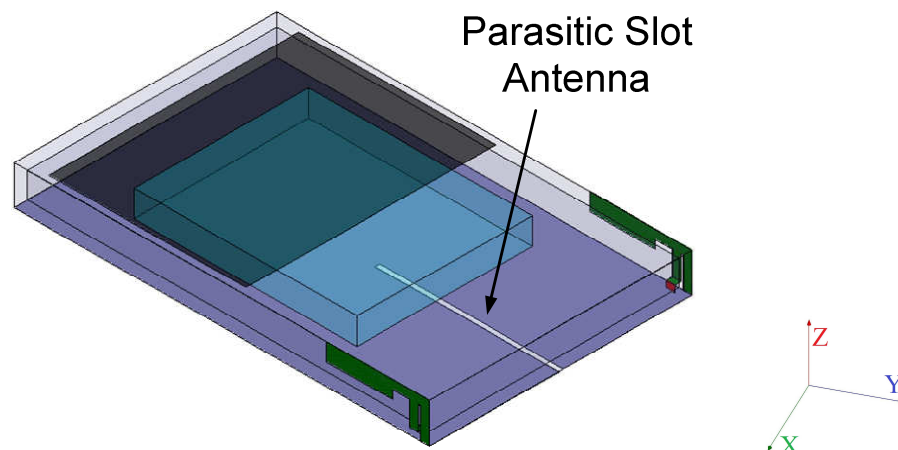


Fig 4.5 The Parasitic Slot Antenna on the GSM-1800 Handset model.

the slot is equal to a quarter of the wavelength (41.6 mm) at 1.8 GHz. The slot is placed in between the two antennas.

The results of the simulations are presented in Table 4.3. The slot antenna succeeds in reducing the mutual coupling between the GSM-1800 MHz antennas to below -15 dB, as required. This however comes at the expense of the bandwidth of the antennas. The bandwidth decreases from 180 MHz to 99 MHz. This in turn means that the antennas, which previously covered both the uplink and downlink bands, must now be retuned so that one antenna covers the uplink while the other antenna covers the downlink band. Figure 4.6 shows the simulated results of this test case. The PIFAs achieve a reflection coefficient of

Table 4.3 Simulated Performance of Antennas for GSM-1800 Handset with and without ground slot radiator

Characteristic	Without Ground Slot (dB)	With Ground Slot (dB)
Reflection Coefficient in Uplink band	$-19.5 < S_{11} < -12.5$ $-19.5 < S_{22} < -12.5$	$-21 < S_{11} < -10.1$ $-7.5 < S_{22} < -4.5$
Reflection Coefficient in Downlink band	$-15.9 < S_{11} < -10.1$ $-15.9 < S_{22} < -10.1$	$-9 < S_{11} < -4.5$ $-16 < S_{22} < -11.5$
Mutual Coupling in Uplink Band	$-10.1 < S_{21} < -9.55$	$-39 < S_{11} < -19$
Mutual Coupling in Downlink Band	$-10.5 < S_{21} < -9.62$	$-21 < S_{11} < -18.5$

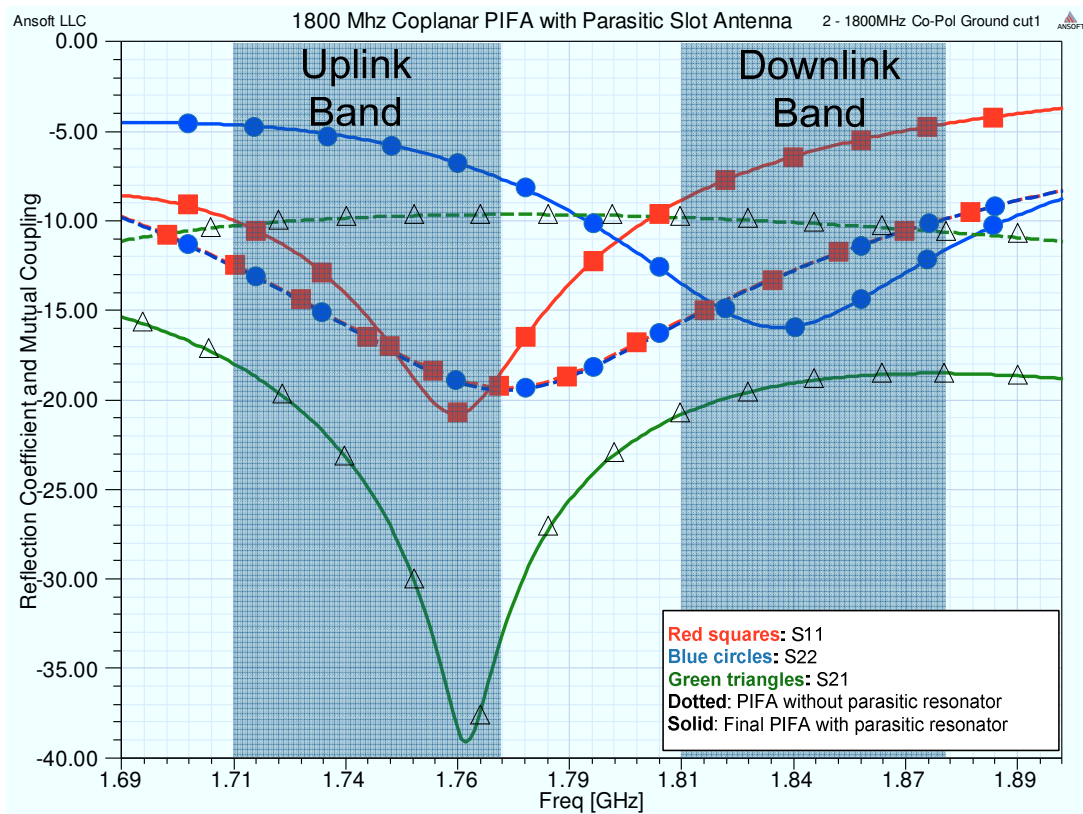


Fig 4.6 The S-Parameters of the GSM-1800 Handset antennas with parasitic radiator.

below -10 dB in their respective bands, while the mutual coupling remains below -15 dB.

4.4.3 Investigation of Electromagnetic Band-Gap Structures for coupling reduction in a Mobile Handset

As indicated earlier in Section 4.2, the EBG design considered in this thesis is a mushroom-type structure with its unit cell composed of a metallic patch (or more in the case of a multi-layer design) connected to the ground plane through a metallic via, as shown in Figure 4.7.

According to Sivenpiper et al. [40] the simple LC circuit, shown in Figure 4.8, can be used to model this mushroom EBG structure for performance predictions. In a mobile handset, a shielding box is used for housing circuit components. An example of this is shown in Figure 4.8. Therefore, the EBG design of Figure 4.6 is inserted in the handset with a metal plate on the top. This is similar to the structure reported in [66] for suppression of noise and wave propagation in lateral

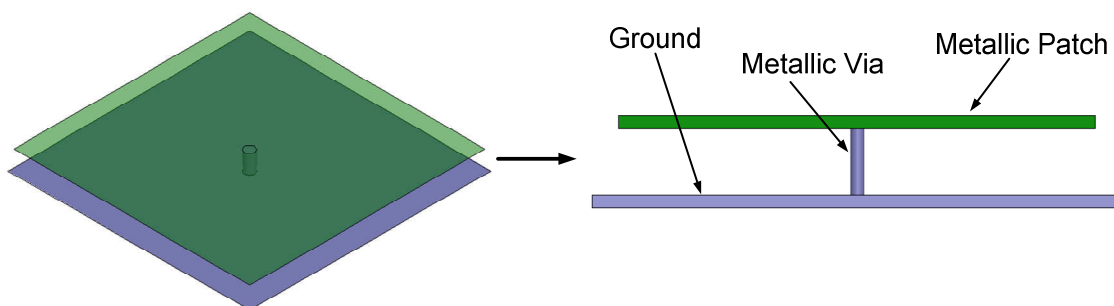


Fig 4.7 The Unit Cell of an Electromagnetic Band-Gap structure. Thickness of items in side-view exaggerated for illustrative purposes.

type EBG structure.

directions, i.e., a 2D band-stop filter. This characteristic can be harnessed in handsets to isolate PIFAs by designing the bandgap (2D stopband) at the operating frequency band of the antennas.

In the studied handset model a new metallic “shielding box” is placed in the interior of the handset which is represented by 35 μm thick copper sheets in the simulations. Figure 4.9 shows an example of a shielding box used in a practical mobile handset. Figure 4.10 shows the resulting EBG unit cell structure for the mobile handset.



Fig 4.9 An example of a metallic shielding box in a mobile handset: the interior of the Apple iPhone 3GS features a metallic shielding box to house the circuit boards. Image source: [70]

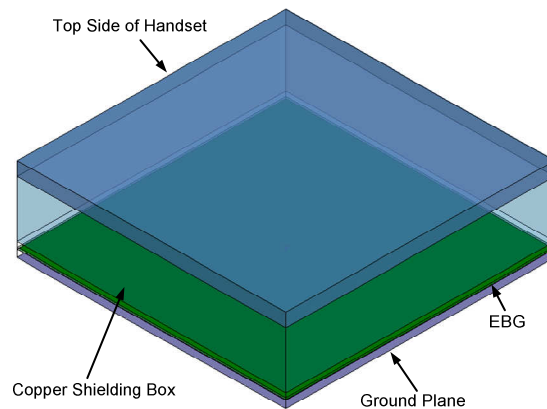


Fig 4.10 The Unit Cell of the Electromagnetic Band Gap Structure for the Mobile Handset.

This EBG unit cell must be small enough to allow for a periodic structure to be set-up in the handset. The authors of [71] concluded that a structure consisting of at least two rows and three columns is required to achieve a stop-band with considerable band rejection characteristics.

Using the guidelines provided by Sievenpiper et al. [40] and Abhari et al. [66], the unit cell of the EBG structure was designed. The initial design featured a ground plane covered with a 1.5 mm thick FR4 substrate. The metallic patch was placed on top of the FR4 substrate (which has a relative permittivity of 4.4). The metallic shielding box was suspended 1 mm on top of the patch and the volume between the patch and shielding box was filled with air (with relative permittivity of 1). The size of this EBG unit cell was 30 mm X 30 mm, which was too large for the considered handset form.

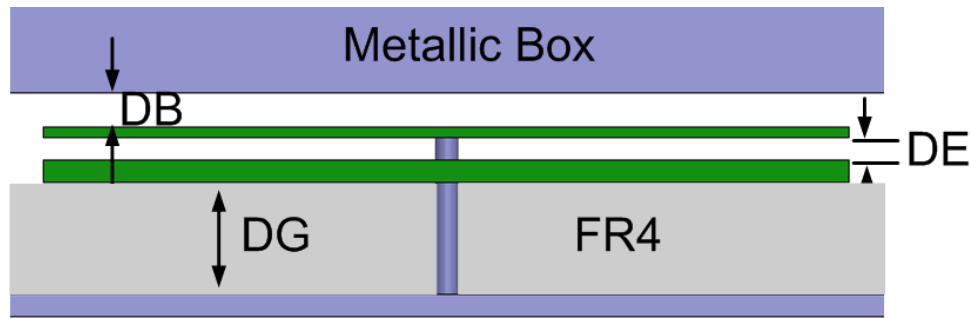


Fig 4.11 Geometrical parameters of the unit cell for the GSM-900/LTE-Band 13 Handsets

Dimensions: $DG=0.75$, $DE=0.2$, $DB=0.75$, patch length and width=28 (all values in mm)

To miniaturize the EBG structure, a second metallic patch is added on top of the first as shown in Figure 4.11. The volume between the first and second

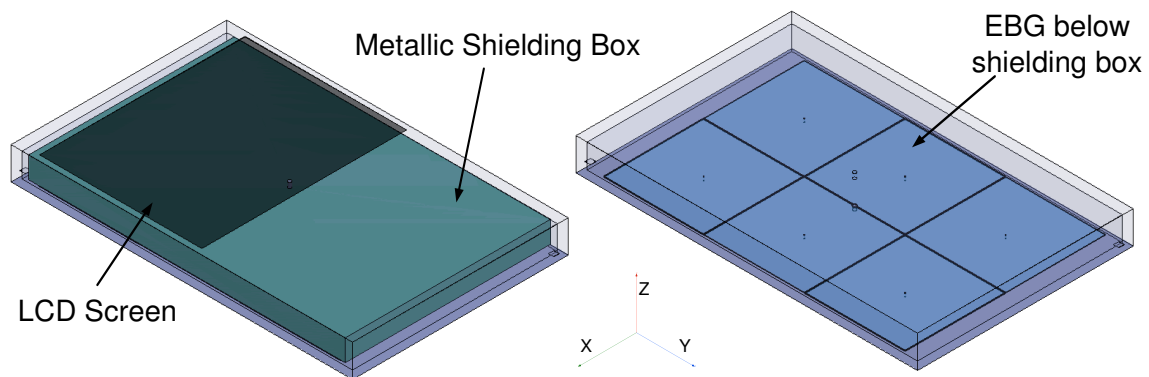


Fig 4.12 The metallic shielding box and the 3 X 2 EBG array placed below it.

patch has the relative permittivity of 1. The final dimensions of the unit cell are 28 mm X 28 mm which is small enough to fit inside the handset in a 3 X 2 array as shown in Fig 4.12.

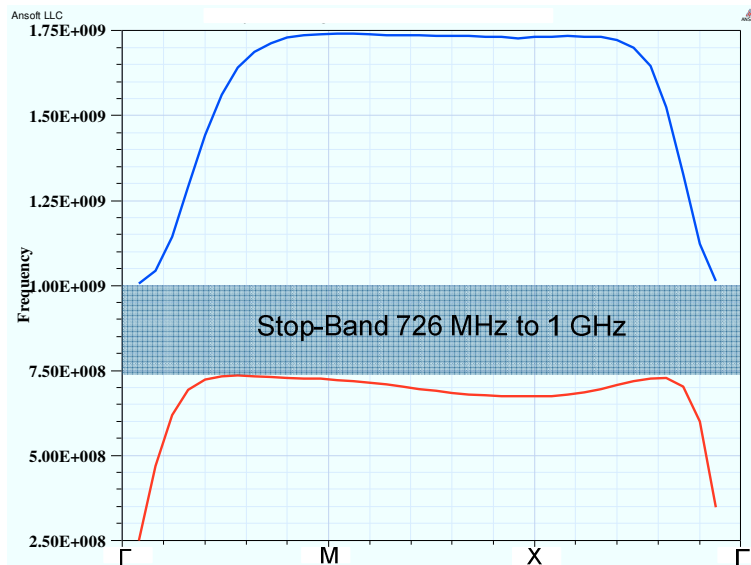


Fig 4.13 Dispersion diagram for the unit cell of the EBG structure shown in Figure 4.10 for the GSM-900/LTE-B13 Handset.

The dispersion diagram of the unit cell, presented in Fig. 4.13, shows that a stop-band extending from 726 MHz to 1 GHz is generated. This is wide enough to cover both the GSM-900 and LTE-Band 13 spectrums.

Placing the metallic shielding box inside the mobile handset volume will affect the radiation characteristics of the antennas as well. Therefore, the PIFAs are first retuned to work in the presence of the shielding box. Once the antennas meet the performance targets (with the possible exception of the mutual coupling), the EBG structure is included in the handset .

The GSM-900 handset is studied first. The simulated S-parameters are shown in Figure 4.14(a) indicating that the EBG structure is not positively

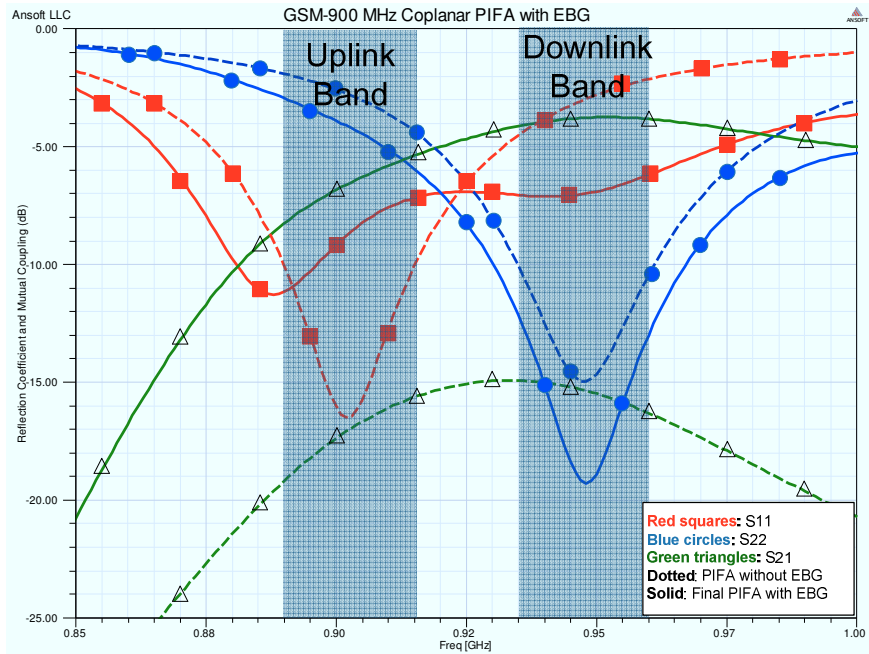
affecting the mutual coupling profile and instead worsening it. This confirms the conclusion in Chapter 3 stating that the antenna coupling in the GSM-900 handset dominantly takes place through space-waves. The decision to not include an EBG array in the GSM-1800 handset stemmed from this rationale and the results for the GSM-900 handset further solidify this reasoning.

In the second case, the LTE-Band 13 handset PIFAs are also retuned to operate in the presence of the shielding box. Figure 4.14(b) shows the change in radiation characteristics with and without the EBG array. The s-parameters for the handset are summarized in Table 4.4. The addition of the shielding box to the handset model alters the reflection coefficients of the PIFAs. The reflection coefficient at the input port of the two antennas remains below the -5 dB design threshold. The mutual coupling exceeds the design limits. After the addition of the EBG array, the reflection coefficient of the antennas is noted to decrease considerably, but remains within the design limits. The mutual coupling decreases from a maximum of -3.9 dB to a maximum of -12.2 dB showing the effectiveness of the EBG structure in increasing antenna isolation.

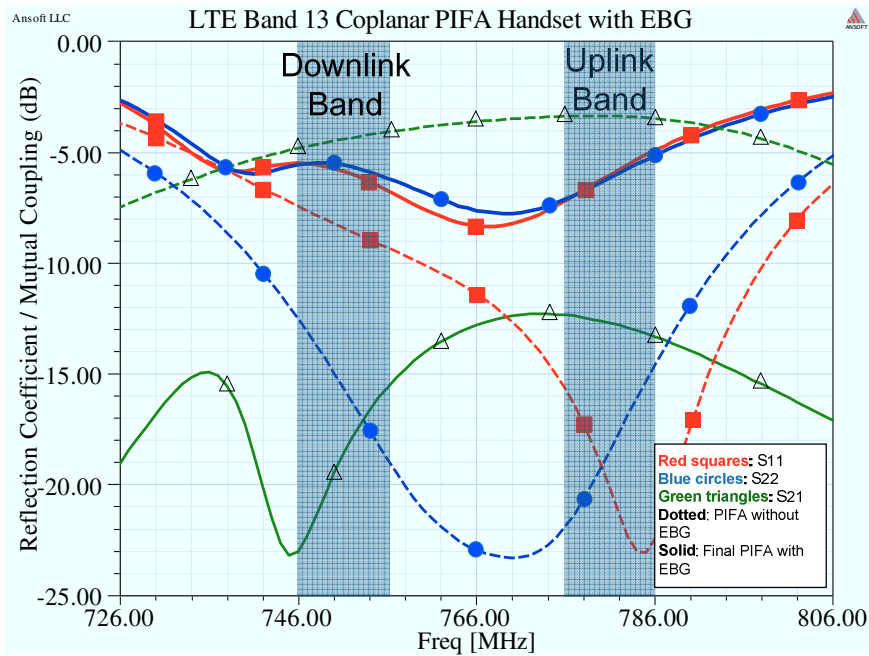
Figure 4.15 shows the radiation patterns of the individual antennas with and without the EBG structures. The addition of the shielding box is noted to alter the reflection coefficients of the antennas in Figure 4.14(b) and causes the gain and efficiencies of the antennas to change as well. The addition of the EBG array to

the handset reduces the gain and efficiencies further. The gain for Antenna #1 reduces from -1.65 dB to -2.8 dB and from -1.45 dB to -2.6 dB for Antenna #2. The efficiency of Antenna #1 changes from 53.4% to 43.1% and from 57.8% to 45.3% for Antenna #2.

The radiation efficiency and gain for the LTE-Band 13 handset continues to depend on the phase difference between the antennas, as shown in Figure 4.16. The relationship between the phase difference and the PIFA-system gain and efficiency is seen in the data listed in Table 4.2. Fortunately, the final design continues to meet the performance targets set for the LTE-Band 13 handset.



(a)



(b)

Fig. 4.14 : The S-parameters for (a) GSM-900 handset with and without the EBG structures (b) LTE-B13 handset with and without the EBG structures.

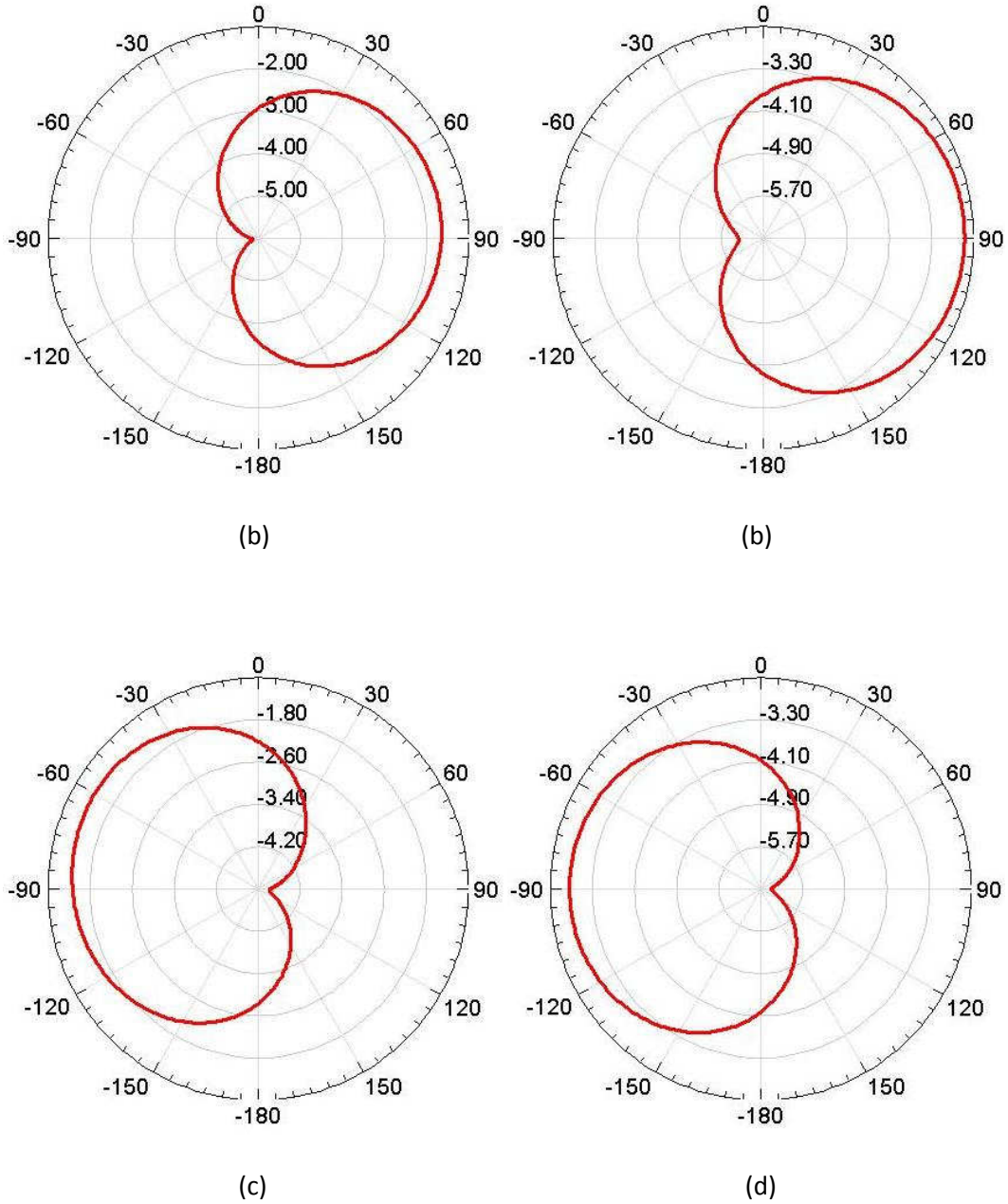


Fig. 4.15 : The radiation pattern of the semi-populated LTE-B13 handset at 766 MHz ($\varphi=0$)
 (a) Simulation result for Antenna #1 without EBG structure (b) Simulated result for Antenna #1 with EBG structure (c) Simulation result for Antenna #2 without EBG structure (d) Simulation result for Antenna #2 with EBG structure.

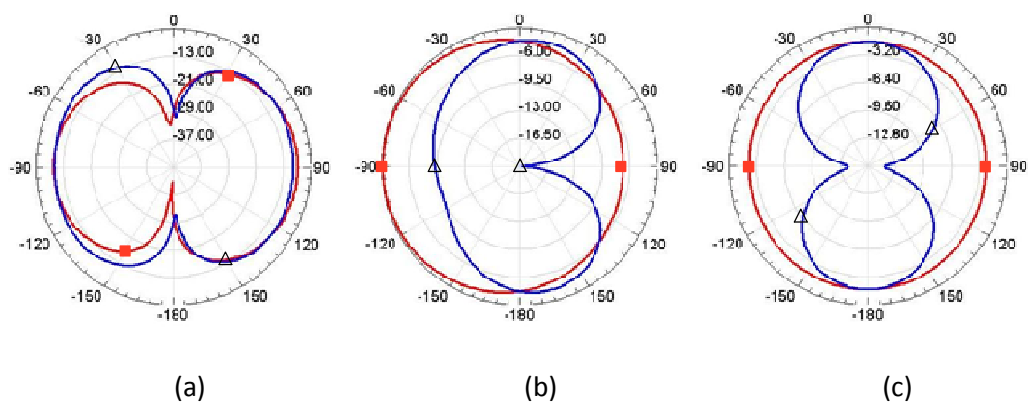


Fig. 4.16 : The radiation patterns of the LTE-Band 13 PIFAs at $\phi=0$ (red square) and $\phi=90$ (blue triangle) planes when the phase difference is: (a) 0 (b) $\pi/2$ (c) π .

Table 4.4 Simulated Performance of Antennas for LTE-B13 Handset with and without EBG structures

Characteristic	Without EBG structure (dB)	With EBG structure (dB)
Reflection Coefficient in Uplink band	$-9.5 < S_{11} < -6.2$ $-19 < S_{22} < -12.4$	$-7 < S_{11} < -5.5$ $-6.2 < S_{22} < -5.6$
Reflection Coefficient in Downlink band	$-23 < S_{11} < -15.7$ $-21.9 < S_{22} < -14.6$	$-7.2 < S_{11} < -5.1$ $-7.2 < S_{22} < -5$
Mutual Coupling in Uplink Band	$-4.5 < S_{21} < -4.1$	$-23 < S_{21} < -15.5$
Mutual Coupling in Downlink Band	$-3.4 < S_{21} < -3.2$	$-13.1 < S_{21} < -12.2$

Table 4.5 Dependence of LTE-Band 13 PIFAs with EBG structure on Phase Difference between Antennas.

Characteristic	Simulated Values (dB)		
	0	$\pi/2$	π
Phase Difference	0	$\pi/2$	π
Max. Gain	-6.8 dB	-2.6 dB	-1.6 dB
Radiation Efficiency	21.4%	67.6%	70%

4.5 Conclusion

This chapter presented a survey of different mutual coupling reduction techniques. A discussion on the most suitable techniques for application on a mobile handset is presented. Techniques that are applicable for the mobile handset are then applied.

First, a coupling reduction method that targets space-wave radiation is investigated. This method uses a parasitic radiator. Two different implementations of the parasitic radiators are presented; a bent monopole and a ground slot antenna. The bent monopole is found to work most effectively for the GSM-900 handset. It succeeded in reducing the mutual coupling but caused the gain and radiation efficiency of the antenna system to drop.

The bent parasitic monopole did not have sufficient bandwidth to lower the mutual coupling across the entire GSM-1800 bandwidth. In order to reduce the antenna coupling in the GSM-1800 handset, a ground slot antenna is suggested. Despite the observed increase in antenna isolation, this approach has the disadvantage of bandwidth reduction along with potential signal and power integrity problems due to a defected ground plane.

The loss of gain and efficiency in the GSM-900 handset, and the loss of bandwidth in the GSM-1800 handset, were both attributed to the disruption of current distribution on the ground plane. The bent parasitic monopole sets up opposing currents that reduce the ability of the ground plane to contribute to the radiation.

To target the antenna coupling via substrate bound modes, an Electromagnetic Band Gap structure is suggested that operates in the presence of a metallic shielding box. The antennas for the models investigated are subsequently modified to work in the presence of the shielding box.

The LTE-Band 13 handset on the other hand showed significant improvement in terms of PIFA isolation. Nevertheless, the EBG filter degraded the overall radiation performance but still met the target operational S-parameter, gain and efficiency values.

Chapter 5

Conclusion

5.1 Thesis Summary

A brief history of mobile handset antenna evolution is presented at the start of this thesis. The discussion concludes that the patch antenna, which is the most widely-used antenna type, is incompatible with the requirements for future MIMO handsets that operate at lower frequency bands. The Printed Inverted-F Antenna (PIFA) is therefore suggested as a suitable alternative and in fact, PIFAs are widely used in today's handsets.

The first detailed investigation of a PIFA-based multi-antenna system for use on a semi-populated mobile handset is then presented at three different telecommunication frequencies; the GSM-900 band, the GSM-1800 band and the LTE-Band 13. A methodology is developed to design the PIFAs to operate on a handset that is populated with a battery and an LCD screen. The presence of these components is shown to deteriorate the antenna performance. Suitable miniaturization techniques are applied to the GSM-1800 and GSM-900 handsets antennas with maximum possible spacing in between. The fabricated model based on the simulated designs for the GSM-1800 handset is able to achieve a reflection coefficient of below -10 dB across the entire operational band, with a

maximum gain of 4.3 dB and 4.26 dB for the two PIFAs. The GSM-900 handset antennas exhibit reflection coefficient values of below -10 dB across both uplink and downlink bands but can only achieve a maximum gain of 0.36 dB and -0.07 dB for its two PIFAs. This drop in gain is attributed to the smaller electrical size of the ground plane at the GSM-900 frequency range.

The two PIFAs of the LTE-Band 13 handset yield reflection coefficient values of below -4.5 dB across both the uplink and downlink bands when operated independently or simultaneously (in a multi-receive mode). The maximum gain of the two-antenna system is found to vary with the phase difference between their inputs.

The mutual coupling in the studied designs at each of the three frequency bands is found to be greater than the desired limits. In order to reduce the coupling, an investigation is carried out using the HFSS Version 12 EM-solver. The software is used to calculate the power flowing through two defined cross-sectional areas: one in the handset and one outside the handset in the space extending from the handset to infinity. The results of the simulations suggest that the power coupled between the antennas in the GSM-1800 and GSM-900 designs is mainly due to the waves propagating through the space outside the handset (space-waves). The LTE-Band 13 handset experiences antenna coupling due to substrate-bound modes inside the handset.

Finally, a survey of different mutual coupling reduction techniques is presented. Using a parasitic radiator, it is shown that the GSM-1800 and GSM-900 handsets do indeed experience coupling due to space-waves. The parasitic radiator, implemented using a ground slot antenna for the GSM-1800 handset, is able to reduce the coupling to below -15 dB across the entire spectrum, as required. The parasitic radiator, in the form of a bent loaded monopole, decreases the coupling to below -15 dB across the entire GSM-900 band, as required.

A coupling reduction technique using Electromagnetic Band-Gap structures (EBG) is investigated at the GSM-900 and LTE-Band 13 frequencies. The EBG structure designed for the GSM-900 handset show no change in the mutual coupling, supporting the conclusion that the antenna coupling for the GSM-900 handset takes place predominantly through space-waves. Nonetheless, the EBG array designed for the LTE-Band 13 handset is able to successfully reduce the mutual coupling below -15 dB across the entire operating spectrum.

5.2 Thesis Conclusions

The main objective of this thesis is to study the feasibility of using Printed Inverted-F Antennas on a 4G mobile handsets at different operating frequencies and to evaluate methods to improve the performance, where necessary.

The first conclusion reached in this thesis is that PIFAs are a strong candidate for use in mobile handsets. The designs for the PIFAs presented in this thesis have thin profiles that can easily be integrated next to other on-board components. They can be mounted on the sides of the handset enabling the designers to utilize the space within the handset more effectively.

The second conclusion is that the performances of the PIFAs are strongly affected by the current distribution on the ground plane. Whenever the electrical size of the ground plane is smaller, as in the case of the GSM-900 or LTE-Band 13 handsets, the radiation performance of the antenna system is degraded. The direction of current distribution is also found to be a performance determining factor, especially in the case of the LTE-Band 13 handset.

The third conclusion is that the mutual coupling between the two antennas takes place through different paths at different frequencies. While the coupling is found to be via space waves for the GSM-1800 and GSM-900 handsets, the PIFA coupling in the LTE-Band 13 handset is found to be caused by handset-bound modes.

The fourth conclusion reached is that the mutual coupling reduction techniques should be selected based on identifying the dominant coupling mechanism. Adding parasitic radiator antenna in the GSM-900 handset is found to be effective in improving antenna isolation. Including a parasitic ground slot

antenna in the GSM-1800 handset and an EBG structure in the LTE-Band 13 handset are found to decrease the PIFA coupling at the pertinent frequency band.

5.3 Future Work

There are different design possibilities that are not investigated due to time constraints. Having provided a mutual coupling profile for the three separate frequency bands in this thesis, future students may wish to investigate what happens when a multi-band antenna is used. The case where a multi-antenna system can cover all three bands will be extremely interesting, given the possibility for multiple coupling paths to exist. The application of more than one mutual coupling reduction technique to the same handset would be an interesting area for further investigation.

The use of multiple parasitic radiators for extending the antenna isolation bandwidth is another area that could be further investigated. The feasibility of implementing a multiple parasitic radiator design on the limited board real estate available in a mobile handset is a design challenge worth studying.

Future handsets are moving towards full-screen LCD models. Handsets using full-screen LCDs will not allow for antennas to be as isolated, as they are in this thesis. Besides impacting the antenna performance, it is possible that a

stronger coupling could occur due to the presence of conductive surface between the antenna and a new coupling profile could emerge. This would require a detailed investigation and would prove to be exceedingly useful.

References

- [1] [Online]. Available: http://www.techfresh.net/wp-content/uploads/2007/09/mobilefirst_5.jpg.
- [2] [Online]. Available: http://img.photobucket.com/albums/v385/Ronaldo_7/nokia-5110.gif.
- [3] [Online]. Available: <http://guide-images.ifixit.net/igi/TALGLxdaNsKhWW6Q.large>.
- [4] [Online]. Available: <http://www.motorolasolutions.com/US-EN/About/Company+Overview/History/Explore+Motorola+Heritage/Cell+Phone+Development>.
- [5] M. Hirose and M. Miyake, "Pattern Control of a $1/4$ Monopole Antenna on a Handset by Passive Loading," in *International Conference on Universal Personal Communications*, Ottawa, 1993.
- [6] S. Sekine and T. Maeda, "The radiation characteristic of a $\lambda/4$ -monopole antenna mounted on a conducting body with a notch [portable telephone model]," in *Antennas and Propagation Society International Symposium*, Chicago, 1992.
- [7] J. Toftgard, S. N. Hornsleth and J. B. Andersen, "Effects on Portable Antennas of the Presence of a Person," *IEEE Transactions on Antennas and Propagation*, vol. 41, no. 6, pp. 739-746, 1993.
- [8] P. Haapala and P. Vainkainen, "Helical antennas for multi-mode mobile phones," in *26th European Microwave Conference*, Prague, 1996.
- [9] I. Egorov and Z. Ying, "A non-uniform helical antenna for dual band cellular phones," in *IEEE Antennas and Propagation Society International Symposium*, Salt Lake City, USA, 2000.
- [10] G. F. Pedersen and J. B. Andersen, "Integrated Antennas for Hand-held Telephones with Low Absorption," in *Proceedings of Vehicular Technology Conference*, Stockholm, pp. 1537-1541, June 1994.
- [11] J. Fuhl, P. Nowak and E. Bonek, "Improved internal antenna for hand-held terminals," *Electronics Letters*, vol. 30, no. 22, pp. 1816-1818, October 1994.
- [12] P. Ciaisi, R. Staraj, G. Kossiavas and C. Luxey, "Design of an Internal Quad-Band Antenna for Mobile Phones," *IEEE Microwave and Wireless Components Letters*, vol. 14, no. 4, pp. 148-150, 2004.
- [13] N. A. Saidatul, A. A. H. Azremi, R. B. Ahmad, P. J. Soh and F. Malek, "Multiband Fractal Planar Inverted F Antenna (F-PIFA) for Mobile Phone Application," *Progress in Electromagnetic*

Research, vol. 14, pp. 127- 148, 2009.

- [14] K. Wong and W. Chen, "Compact Microstrip Antenna with dual-band frequency operation," *Electronics Letters*, vol. 33, no. 8, pp. 646-647, 1997.
- [15] Z. D. Liu, P. S. Hall and D. Wake, "Dual-Frequency Planar Inverted-F Antenna," *IEEE Transactions on Antennas and Propagation*, vol. 45, no. 10, pp. 1451-1458, October 1997.
- [16] B. F. Wang and T. Y. Lo., "Microstrip Antennas for Dual-frequency Operation," *IEEE Transactions on Antenna and Propagation*, vol. 32, no. 9, pp. 938-943, September 1984.
- [17] A. K. Shrivervik, J. F. Zurcher, O. Staub and J. R. Mosig, "PCS Antenna Design: The Challenge of Miniaturization," *IEEE Antennas and Propagation Magazine*, vol. 43, no. 4, pp. 12- 27, August 2002.
- [18] J. Huang, A Review of Antenna Miniaturization Techniques for Wireless Applications, California Institute of Technology: Jet Propulsion Laboratory, 2001.
- [19] R. B. Waterhouse, S. D. Targonski and D. M. Kokotoff, "Design and Performance of Small Printed Antennas," *IEEE Transactions on Antennas and Propagation*, vol. 46, no. 11, pp. 1629-1633, November 1998.
- [20] H. Chattha, Y. Huang and Y. Lu, "PIFA Bandwidth Enhancement by Changing the Widths of Feed and Shorting Pins," *IEEE Antennas and Wireless Propagation Letters*, vol. 8, pp. 637-640, 2009.
- [21] B. C. K. Kim, J. D. Park and H. D. Choi, "Tapered Type PIFA Design for Mobile Phones at 1800 MHz," in *The 57th Annual IEEE semiannual Vehicular Technology Conference*, April 2003.
- [22] F. Wang, Z. Du, Q. Wang and K. Gong, "Enhanced-bandwidth PIFA with T-shaped ground plane," *Electronics Letters*, vol. 40, no. 23, pp. 1504-1505, November 2004.
- [23] M. R. Islam and M. Ali, "Ground Current Modification of Mobile Terminal Antennas and Its Effects," *IEEE Antennas and Wireless Propagation Letters*, vol. 10, pp. 438-441, 2011.
- [24] A. H. Kusuma, A. Sheta, I. Elshafiey, M. Alkanhal, S. Aldosari, Z. Siddiqui and S. A. Alshebeili, "A Novel Low SAR PIFA for Mobile Terminal," in *IEEE 21st Symposim on Personal Indoor and Mobile Radio Communications* , Istanbul, 2010.
- [25] [Online]. Available: <http://crackberry.com/storm2-teardown-get-good-look-touchscreens-heart-and-soul>.
- [26] S. Parkvall, E. Englund, A. Furskar, E. Dahlman, T. Jonsson and A. Paravati, "LTE Evolution

towards IMT-Advanced and Commercial Network Performance," in *IEEE International Conference on Communication Systems (ICCS)*, Singapore, 2010.

- [27] "ITU4G," [Online]. Available: http://www.itu.int/net/pressoffice/press_releases/2010/48.aspx.
- [28] A. K. Shackelford, S. Y. Leong and K. F. Lee, "Small-Size Probe-Fed Notched Patch Antenna with a Shorting Post," *Microwave and Optical Technology Letters*, vol. 31, no. 5, pp. 377-379, 2001.
- [29] K.-L. Wong, "Modified Planar Inverted-F Antenna," *Electronics Letters*, vol. 34, no. 1, pp. 7-8, 1998.
- [30] P. N. Fletcher, M. Dean and A. R. Nix, "Mutual Coupling in multi-element array antennas and its influence on MIMO channel capacity," *Electronics Letters*, vol. 39, no. 4, pp. 342-344, February 2003.
- [31] C. A. Balanis, *Antenna Theory and Design*, Wiley, 2005.
- [32] C. Soras, M. Karaboikis, G. Tsachtsiris and V. Makios, "Analysis and Design of an Inverted-F Antenna Printed on a PCMCIA Card for the 2.4 GHz ISM Band," *IEEE Antenna and Propagation Magazine*, vol. 44, no. 1, pp. 37-44, February 2002.
- [33] W. Geyi, Q. Rao, S. Ali and D. Wang, "Handset Antenna Design: Practice and Theory," *Progress in Electromagnetics Research*, pp. 123-160, 2008.
- [34] Z. Ying and D. Zhang, "Study of the mutual coupling, correlations and efficiency of two PIFA antennas on a small ground plane," in *IEEE Antennas and Propagation Society International Symposium*, 2005.
- [35] A. C. K. Mak, C. R. Rowell and R. D. Murch, "Isolation Enhancement Between Two Closely Packed Antennas," *IEEE Transactions on Antennas and Propagation*, vol. 56, no. 11, pp. 3411-3419, November 2008.
- [36] J.-G. Yook and L. Katehi, "Micromachined microstrip patch antenna with controlled mutual coupling and surface waves," *IEEE Transactions on Antennas and Propagation*, vol. 49, pp. 1282-1289, September 2001.
- [37] M. M. Nikolic, A. R. Djordjevic and A. Nehorai, "Microstrip Antennas With Suppressed Radiation in Horizontal Directions and Reduced Coupling," *IEEE Transactions on Antennas and Propagation*, vol. 53, no. 11, pp. 3469-3476, November 2005.
- [38] M. Sonkki and E. Salonen, "Low Mutual Coupling Between Monopole Antennas by Using two slots," *IEEE Antennas and Propagation Letters*, vol. 9, pp. 138-141, 2010.

- [39] F.-G. Zhu, J.-D. Xu and Q. Xu, "Reduction of Mutual Coupling between closely-packed antenna elements using defected ground structure," *Electronics Letters*, vol. 45, no. 12, pp. 601-602, 2009.
- [40] D. Sievenpiper, L. Zhang, R. F. J. Broas, N. G. Alexopolous and E. Yablonovitch, "High-Impedance electromagnetic surfaces with a forbidden frequency band," *IEEE Transactions on Microwave Theory*, vol. 47, pp. 2059-2074, November 1999.
- [41] R. King, C. W. Harrison and D. H. Denton, "Transmission-Line Missile Antennas," *IRE Transactions on Antennas and Propagation*, vol. 8, no. 1, pp. 88-90, January 1960.
- [42] L. Pazin and Y. Leviatan, "Inverted-F Laptop Antenna With Enhanced Bandwidth for Wi-Fi/WiMAX Applications," *IEEE Transactions on Antennas and Propagation*, vol. 59, no. 3, pp. 1065-1068, March 2011.
- [43] M. Ali and G. J. Hayes, "Small Printed Integrated Inverted-F Antenna for Bluetooth Application," *Microwave and Optical Technology Letters*, vol. 33, no. 5, pp. 347-349, June 2002.
- [44] C. R. Rowell, "A Capacitively Loaded PIFA for compact PCS Handsets," in *Antennas and Propagation Society International Symposium*, Baltimore, 1996.
- [45] "Ansoft HFSS," Ansys Inc., [Online]. Available: <http://www.ansys.com/Products/Simulation+Technology/Electromagnetics/High-Performance+Electronic+Design/ANSYS+HFSS>.
- [46] K. L. Wong, *Planar Antennas for Wireless Communications*, New York: Wiley, 2003.
- [47] W. L. Stutzman and G. A. Thiele, *Antenna Theory and Design*, Wiley, 1997.
- [48] [Online]. Available: <http://www.globallaminates.com/>.
- [49] [Online]. Available: <http://www.etsi.org/WebSite/Technologies/Cellularhistory.aspx>.
- [50] [Online]. Available: <http://www.3gpp.org/specifications>.
- [51] [Online]. Available: <http://www.3gpp.org/LTE>.
- [52] A. Boag and A. Boag, "Reduction of Mutual Coupling by Near-Field Coupled Resonators," in *IEEE Conference on Microwaves, Communications, Antennas and Electronics Systems*, Tel Aviv, 2009.
- [53] D. M. Pozar, *Microwave Engineering*, Wiley, 2004.

- [54] J.-P. Daniel, "Mutual Coupling Between Antennas for Emission or Reception - Application to Passive and Active Dipoles," *IEEE Transactions on Antennas and Propagation*, vol. 22, no. 2, pp. 347-349, March 1974.
- [55] D. R. Jackson, J. T. Williams, A. K. Bhattacharyya, R. L. Smith, S. J. Buchheit and S. A. Long, "Microstrip Patch Designs That Do Not Excite Surface Waves," *IEEE Transactions on Antennas and Propagation*, vol. 41, no. 8, pp. 1026-1037, August 1993.
- [56] A. Suntives and R. Abhari, "Design of a Compact Minaturized Probe-Fed Patch Antenna Using Electromagnetic Bandgap Structures," in *IEEE International Symposium on Antenna and Propagation*, July 2010.
- [57] D. M. Pozar, "Microstrip antenna aperture-coupled to a microstripline," *Electronics Letters*, vol. 21, no. 2, pp. 49-50, January 1985.
- [58] Z. N. Chen, F. Yang and T. S. P. See, "Mutual Coupling between Multi-band Antennas on Small Ground Plane," in *Fourth European Conference on Antennas and Propagation*, Barcelona, 2010.
- [59] M. N. D. Sadiku, *Elements of Electromagnetics*, New York: Oxford University Press, 2007.
- [60] Y. Yao, X. Wang and J. Yu, "Multiband Planar Monopole Antenna for LTE MIMO Systems," *International Journal of Antennas and Propagation*, 2012.
- [61] B. K. Lau and J. B. Andersen, "Simple and Efficient Decoupling of Compact Arrays with Parasitic Scatterers," *IEEE Transactions on Antennas and Propagation*, vol. 60, no. 2, pp. 464-472, 2012.
- [62] J. G. Yook and L. Katehi, "Micromachined Microstrip Patch Antenna With Controlled Mutual Coupling and Surface Waves," *IEEE Transactions on Antennas and Propagation*, vol. 49, pp. 1282-1289, 2001.
- [63] J.-Y. Chung, T. Yang, J. Lee and J. Jeong, "Low correlation MIMO antenna for LTE 700MHz band," in *IEEE International Symposium on Antennas and Propagation*, Spokane, 2011.
- [64] J. Kim, M. Kim and S. Jeon, "Dual-Antenna diversity-gain improvements for even-odd mode feed network at 755 MHz," *Microwave and Optical Technology Letters*, vol. 53, no. 2, pp. 304-306, 2011.
- [65] I. D. Dioum, A. Luxey and C. Farsi, "Compact Dual-Band Monopole Antenna for LTE Mobile Phones," in *Loughborough Antennas and Propagation Conference*, 2010.
- [66] R. Abhari and G. V. Eleftheriades, "Metallo-dielectric electromagnetic bandgap structures for suppression and isolation of the parallel-plate noise in high-speed circuits," *IEEE Transactions*

on Microwave Theory and Techniques, vol. 51, no. 6, pp. 1629-1639, June 2003.

- [67] J. R. Sohn, K. Y. Kim and H.-S. Tae, "Comparitive Study on Various Artificial Conductors for Low-Profile Antenna," *Progress in Electromagnetics Research*, 2006.
- [68] K. Payandehjoo and R. Abhari, "Employing EBG Structures in Multiantenna Systems for Improving Isolation and Diversity Gain," *IEEE Antennas and Propagation Letters*, vol. 8, pp. 1162-1165, 2009.
- [69] K. Payandehjoo and R. Abhari, "Investigation of Parasitic Elements for Coupling Reduction in Multi-Antenna Hand-Set Devices," *International Journal of RF and Microwave Computer-Aided Engineering*, Awaiting Publication.
- [70] [Online]. Available: <http://guide-images.ifixit.net/igi/rCCm5AE66SuiUi2C.medium>.
- [71] J. Itoh, N. Michisita and H. Morishita, "A Study on Mutual Coupling Reduction Between Two Inverted-F Antennas Using Mushroom Type EBG Structures," in *IEEE Antennas and Propagation Society International Symposium*, San Diego, 2008.
- [72] H. Li, Y. Tan, B. K. Lau, Z. Ying and S. He, "Characteristic Mode Based Tradeoff Analysis of Antenna-Chassis Interactions on Multiple Antenna Terminals," *IEEE Transactions on Antennas and Propagation*, vol. 60, no. 2, pp. 490-502, February 2012.
- [73] C.-Y. Chiu, C.-H. Cheng, R. D. Murch and C. R. Rowell, "Reduction of Mutual Coupling Between Closely-Packed Antenna Elements," *IEEE Transactions on Antennas and Propagation*, vol. 55, no. 6, pp. 1732-1738, June 2007.
- [74] S. Zhang, S. N. Khan and S. He, "Reducing Mutual Coupling for an Extremely Closely-Packed Tunable Dual-Element PIFA Array Through a Resonant Slot Antenna Formed In-Between," *IEEE Transactions on Antennas and Propagation*, vol. 58, no. 8, pp. 2771-2776, 2010.